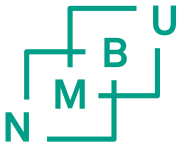

Norwegian University of Life Sciences
Department of Mathematical Sciences and Technology

Master thesis 2014
60 credits

Numerical Stability of a Scalar Neural-Field Model with a Sigmoidal Firing-Rate Function.

Bjørn Mikkel Elle Lepperød

Preface

Applied mathematics and neuroscience have fascinated me greatly for over three years. The self-ordering in nature is highly evident in biological systems and it seems impossible not be amazed by how our brain consists of self aware chunks of atoms (cells). The language of mathematics can hopefully capture some of the interesting aspects in how this is to be. However, if the mathematical models are not 'well behaved', one might endorse dynamics with no foundation in reality. At the same time if the mathematical modeling procedure removes to much physical details, then one might end up with the same problematic endorsement. By narrowing the gap between pure theoretical and experimental sciences, and letting these two philosophical fields inspire one another, I believe the next great insight in the physical sciences can rise. These are some of my major motivations to learn more about rigorous mathematical analysis and finally embark on my master thesis.

In the progress of writing this thesis I have been fortunate to have two excellent supervisors: Prof. John Andreas Wyller and Prof. Bjørn Fredrik Nielsen. They have both been a major inspiration and they have kept my focus in the right direction throughout my masters.

Abstract

Many neural-field models in neuroscience mimic the all or nothing behavior of a neuron firing an action potential. The neural-field model considered in this study is a spatio-temporal scalar neural-field (NFL) model given as a partial integro differential equation (PIDE). The model yields temporal changes in probability of neural activity in a given spatial point. A point has a high probability of activity when the solution of the NFL model is above a firing threshold. The sensitivity to change in probability is measured by a steepness parameter β.

Various numerical methods have been employed on this (and similar) type(s) of neural-field model(s) without analysis of numerical convergence, stability and consistency. The aim of this thesis is to obtain a better understanding of the NFL model's well-posedness theory and its biophysical background. Further to analyze the numerical convergence theory of the NFL model approximated by simple explicit numerical methods.

To obtain a comprehensive overview of the NFL model, we review its biophysical derivation and discuss two proposed formalisms with respect to numerical analysis and well-posedness theory. Further, we review a global well-posedness proof of the Cauchy formulated NFL model in a Banach space of continuous functions. We further perform an analysis of the numerical error obtained in the forward Euler and Heun's second order Runge–Kutta (RK2) method. Finally we illustrate numerical behavior by experiments applying the forward Euler and an explicit RK4 method.

Presented analytical work indicate stiffness (a necessity for a significantly small temporal stepping length) in the NFL model when approximated by the forward Euler method. This is due to a dependency between the numerical error and the steepness parameter β. The RK2 truncation error contains β^2, indicating that β^N is contained in the RKN truncation error. Thus, by increasing the order of the RK method, we predict no remedy with respect to stiffness.

Performed numerical experiments on a simplified version of the NFL model demonstrate stiffness in the proximity of the firing threshold for moderately sized steepness parameters β. We further demonstrate a divergence between the exact and the approximated solution of a slightly less simplified version of the NFL model. This happens when the approximated solution is shifted from one basin of attraction to another, giving rise to a large numerical error. In addition, we observe spurious solutions in the form of false oscillations and an erroneous fixed point. Thus indicating a possibility for numerical solutions of the NFL model to be rather arbitrary when the temporal stepping lengths are not carefully selected.

Presented results indicate serious numerical stability issues in the NFL model. We suggest further evaluation and development of more sophisticated numerical methods for future application of this (and similar) type(s) of neural-field model(s). Finally, we argue the simplicity of the NFL model to be undermined by the complications observed in numerical approximations. We propose focus to be directed towards developing more robust field-models with respect to numerical analysis rather than developing more complicated numerical methods.

Sammendrag

Mange matematiske modeller i nevrovitenskap innehar beskrivelsen av av/på prosessen i nevral fyring av aksjonspotensialer. Nevrofeltmodellen studert i denne tesen er en rom-temporal, skalar nevrofelt (NFL) modell gitt som en partiell integro differensialligning (PIDE). Modellen gir temporal endring av sannsynlighet for nevral aktivitet i et gitt romlig punkt. Et punkt har høy sannsynlighet for aktivitet hvis løsningen av NFL modellen er høyere enn en gitt fyringsterskel. Sensitiviteten til endringer i sannsynlighet er gitt ved en bratthetsparameter β.

Flere numeriske metoder er anvendt på denne, og lignende type nevrofeltmodeller, uten analyse av numerisk stabilitet, konvergens eller konsistens. Målet med denne oppgaven er dermed å få en bedre forståelse av modellens etablerte biofysiske utledning samt eksistens– og unikhetsteori. Videre, å analysere numerisk konvergensteori for enkle eksplisitte numeriske metoder brukt til å approksimere NFL modellen.

For å få en god bakgrunnforståelse av modellen gjennomgår vi en etablert biofysisk utledning og diskuterer to mulige formalismer anvendt på NFL modellen. Videre gjennomgår vi et bevis for global velformulerthet av den Cauchy formulerte NFL modellen i et Banach rom av kontinuerlige begrensede funksjoner. Vi utleder trunkeringsfeilen og den numeriske feilen for den eksplisitte Euler metoden. Videre utledes trunkeringsfeilen til Heun's andre ordens Runge–Kutta (RK2) metode og numeriske eksperimenter blir utført med den eksplisitte Euler metoden og en eksplisitt RK4 metode.

Det presenterte analytiske arbeidet indikerer at NFL modellen er 'stiv' (behøver signifikant redusert verdi av numerisk steglengde) i nærheten av fyringsterskelen. Den indikerte stivheten er hovedsakelig forårsaket av en avhengighet til bratthetsparameteren β i den numeriske feilen til den eksplisitte Euler metoden. Videre innehar trunkeringsfeilen for RK2 metoden bratthetsparameteren β^2. Dette indikerer at trunkeringsfeilen til RKN metoder kan være avhengige av β^N og dermed at stivheten vil være signifikant i alle eksplisitte RK metoder.

Numeriske eksperimenter av en forenklet versjon av NFL modellen demonstrerer stivhet i nærheten av fyringsterskelen ved moderate størrelser av bratthetsparameteren. Videre vises et scenario hvor en approksimasjon divergerer fra den eksakte løsningen av en mindre forenklet versjon av NFL modellen. Dette skjer da approksimasjonen blir flyttet fra et tiltreknings-område til et annet. I tillegg observerer vi falske oscillasjoner og et falskt fiks-punkt generert av numerisk feil. Dette viser at numeriske approksimasjoner av NFL modellen kan være tilfeldige hvis ikke den temporale steglengden velges med omhu.

Den rom-temporale NFL modellen indikeres til å inneha alvorlige stabilitets-problemer som viser at det behøves grundig analyse som forhåndsregel ved bruk av numeriske metoder på denne modellen. Avslutningsvis argumenteres det for fokus på utvikling av mer robuste feltmodeller i forhold til numerisk approksimering. Dette fordi enkeltheten ved approksimasjon av NFL modellen undergraves av den indikerte stivheten.

Contents

1 Introduction **1**

2 The NFL model in neuroscience **3**
2.1 The neuron . . . 3
2.2 Derivation of the NFL model . . . 3
2.3 PDE versus ODE formalism . . . 6

3 The well-posedness of the NFL model **7**
3.1 Assumptions . . . 7
3.2 Volterra formulation . . . 8
3.3 Stability . . . 13

4 Numerical analysis **15**
4.1 Definitions . . . 15
4.2 Preliminary analysis . . . 16
4.3 Forward Euler approximation . . . 18
4.3.1 Consistency . . . 18
4.3.2 Convergence . . . 19
4.4 Heun's second order Runge–Kutta method . . . 21
4.4.1 Consistency . . . 22

5 Results and discussion **25**
5.1 The firing-rate function . . . 25
5.2 Numerical stability of the forward Euler method . . . 26
5.3 Numerical experiments on a spatially independent model . . . 28
5.3.1 Local error . . . 28
5.3.2 Convergence estimate in the proximity of the firing threshold . . . 30
5.3.3 Theoretical estimates versus numerical experiments . . . 32
5.3.4 Unstable equilibrium points . . . 33
5.3.5 Global error . . . 34
5.4 Numerical experiments on a coupled pair model . . . 35

6 Concluding remarks and outlook **40**
6.1 Concluding remarks . . . 40
6.2 Outlook . . . 40

Appendix A Pseudo exact solution **42**
A.1 Derivation . . . 42
A.2 Stability of the spatial independent NFL model . . . 43
A.3 Asymptotes of the spatial independent NFL model . . . 44

Appendix B Theorems and definitions **46**
B.1 The contraction mapping theorem . . . 46
B.2 Differentiation of integral equations . . . 46
B.3 Mean value theorem for integrals . . . 47
B.4 Mean value theorem . . . 47
B.5 Taylors theorem . . . 47
B.6 Lipschitz continuity . . . 47

Appendix C Python code **48**
C.1 Convergence estimates of a spatially independent model . . . 48
C.2 Nonlinear curve fit . . . 48
C.3 System of two populations . . . 49

1 Introduction

In vertebrates, the central nervous system is located in the spinal cord and the brain, where the former is believed to be the main processing unit. The brain is divided in several sections which are believed to be connected to specific working tasks. The cortex is a major section in higher mammals and is observed to be larger in species associated with higher intelligence, being the largest in the human brain. Nerve cells in the central nervous system are termed as neurons and are believed to be the main information processors and transmitters. One nerve cell is of finite size and has individual functionality which is mathematically well-described, much due to the success of Hodgkin and Huxley (1952). Today, the greatest challenge is to decipher how the neurons are functioning in a network as to better understand the complexity of the brain. Modeling approaches on neural networks are generally separated by the amount of biophysical details contained in the model; see e.g. Sterratt et al. (2011) for a comprehensive review.

One approach in describing neural networks is found in the neural field models. These are some of the simplest network models with regard to biophysical details and aim to describe the macroscopic dynamics of networks of neurons. The brain tissue of higher mammals have a high density of neurons where the coupling junctions between neurons, called synapses, appears to be randomly connected. Neuronal signals can reach centimeters into the brain tissue, a distance much larger than the size of a single neuron. Thus indicating that macroscopic activity in groups of neurons can be described as a continuum, or so called neural fields Coombes (2006). Experimental motivation for the continuum approximation can be found e.g. in the rodent whisker system. Here it is observed specific mappings of neural populations to whiskers, i.e., when a whisker is deflected, the response is directed to a specific neural population in the primary sensory area. After a few milliseconds the direct response in a population propagates out to a multitude of other populations with complex spatiotemporal dynamics (Petersen, 2007). In an attempt to describe these observations mathematically, it is assumed that the populations of neurons can be regarded as a neural 'signal field' propagating the signals through nearby brain tissue (Bressloff, 2012)[p. 185]. A population in neural fields is considered as a pool of homogeneous neurons squeezed together, where the macroscopic state variables are the mean firing rate of each population (Coombes, 2005). In the primary sensory area of rodents these pools of neurons reflect observed micro- and macro columns of neurons (Coombes, 2006), thus endorsing the neural field description.

The spatio-temporal scalar neural-field (NFL) model studied in this thesis is presented as

$$\begin{aligned} &\frac{\partial}{\partial t}u(x,t) = -u(x,t) + \int_{\Omega} \omega(x,x')S_\beta(u(x',t)-u_\theta)\,\mathrm{d}x', \quad && t>0 \\ &u(x,t) = u_0(x), && t=0. \end{aligned} \tag{1.1}$$

Here $x \in \Omega$, where Ω is a bounded subset of $\mathbb{R}$, ω denotes a weighting function used to describe the connectivity between populations of neurons, termed the *connectivity function*. When $\omega(x,x')$ is positive (resp. negative), the connectivity is termed excitatory (resp. inhibitory). A smooth non linear *firing-rate function* is denoted as S_β. The firing-rate function approaches the Heaviside step function as $\beta \to \infty$, where β measures the steepness of the firing-rate function. In the succeeding text β is termed the *steepness parameter*. The firing-rate function gives the probability densities for a neuron population to be in an active state (the neurons are either 'on' or 'off'). This probability is usually modeled by a sigmoidal, a piecewise continuous or a Heaviside step function, all saturating at 0 and 1. The firing rate function yield high probability for activity if the solution $u(x',t)$ is larger than the parameter u_θ denoting the threshold value for activity, termed as *the firing threshold*.

The first studies in neural field theory provided very simple models where only excitation and no refractoriness was considered (see Section 2 for an explanation of the terms). The mathematicians Wilson and Cowan (1972, 1973) were the first to include inhibitory neurons and refractoriness in the model. In further studies by Amari (1975, 1977) pattern formations were studied in the NFL model by approximating the firing-rate function with a Heaviside step function. He reported that the NFL model have five types of pattern dynamics when applying a lateral inhibitory (local excitation and distant inhibition) connectivity function. More recent studies have focused on generic features: generation and stability of structures such as spatially localized stationary solutions (bumps), spatially or spatiotemporally oscillating patterns and traveling waves, pulses and fronts; see e.g. Ermentrout (1998); Coombes (2005) and the references therein. These mathematical features have been connected

to phenomenas such as short-term memory, the head direction system, visual hallucinations, and EEG rhythms; see Coombes (2005) and the references therein.

In addition to study pattern formation, Amari (1977) conjectured structural stability of the NFL model, suggesting that the Heaviside step function ($\beta \to \infty$) approximates the smooth firing-rate function ($\beta < \infty$). In an attempt to support this argument Oleynik et al. (2013) rigorously justified that stationary solutions of the NFL model with $\beta < \infty$ converges to stationary solutions when $\beta \to \infty$. Although, Nielsen et al. (2013) demonstrated ill-posedness of the NFL model in the sense of Hadamard when $\beta \to \infty$, by demonstrating a discontinuous initial condition to solution map. Examples of stationary solutions with $\beta < \infty$ vanishing in the $\beta \to \infty$ limit was given. Further, the NFL model was proved stable with $\beta < \infty$, i.e. continuous initial conditions and steepness parameters to solution maps. The limit $\beta \to \infty$ is therefore not taken into consideration in this thesis.

There is a need for solving the NFL model using computational approaches as the firing-rate function is nonlinear and the model is non-local. Various numerical methods have been employed when analyzing these types of neural-field models (see e.g. Coombes and Schmidt (2010)) without accounting for numerical convergence, stability and consistency. However, an exception is found in Faye and Faugeras (2010), where a consistent numerical scheme was derived by the trapezoidal rule on a delay version of the NFL model. Although, there were given no justifications on the selected temporal stepping lengths. As argued by Nielsen et al. (2013), the NFL model is only 'theoretically' stable. Hence, conjecturing numerical approximations to produce erroneous results if arbitrary temporal stepping lengths are employed in e.g. Euler and Runge–Kutta (RK) methods. In addition, they conjectured that changing the order of the RK method does not yield results with a higher accuracy since the higher order temporal derivatives of the NFL model are indicated to contain the steepness parameter.

The NFL model is a continuum of ordinary differential equations (ODEs) parametrized by the spatial coordinates; see the end of Section 2. Therefore, to study this model, theory from ODEs can provide well understood tools for theoretical and numerical analysis. A different approach have emerged from e.g. studies of wave fronts (Ermentrout and McLeod, 1993) induced in the NFL model. This approach consist of re-casting the model as a higher order nonlinear partial differential equation (PDE) by means of Fourier transforms; see e.g. Laing and Troy (2003); Coombes (2005). However, this approach imposes serious restrictions on the connectivity kernel making the model less general. In addition, the PDE formalism represents a complex field of mathematical theory which can be avoided by the ODE approach.

The aim of this thesis is therefore to review a biophysical derivation and a proof of well-posedness, to get a comprehensive overview of the NFL model. Analyze convergence, consistency and stability of given explicit numerical methods when employed on the NFL model. We employ standard explicit numerical methods to evaluate numerical behavior of the NFL model. However it is not known to the author any previous studies which have employed the methods used in this study on the NFL model. Therefore, in the following, we detail the aims which are believed to be a contribution to the field of neural-field models. We discuss an ODE versus a PDE approach in analyzing the NFL model, with respect to well-posedness theory and numerical approximations. The numerical convergence and consistency of the NFL model solved by the forward Euler method are addressed. Further, consistency of Heun's RK2 method is assessed and the truncation errors of the forward Euler and Heun's RK2 method are to be compared towards numerical efficiency of these methods. Note that Faye and Faugeras (2010) studied a temporal delay version of the NFL model and assessed consistency of the trapezoidal method which is similar to Heun's RK2 method. However without focus on the temporal stepping length, which is a focus in this thesis. An analytical analysis of stability with respect to the forward Euler method is performed. Stability of an explicit RK4 method applied on the NFL model is addressed by numerical experiments. The types of numerical errors occurring in the forward Euler and a explicit RK4 method i.e. round off, local and global errors will be discussed. Finally in an outlook we discuss the prospects of the NFL model with respect to numerical approaches and the models future place in neuroscience.

2 The NFL model in neuroscience

2.1 The neuron

The following introductional description of the neuron is adapted from Gerstner and Kistler (2002)[ch. 1].

A neuron consists of dendrites, a soma, an axon and synapses; see Fig. 1. Dendrites collect signals and transmit them to the soma. A nonlinear process is performed in the soma, where a signal called an action potential is fired if the total input exceeds a firing threshold. This signal is a result of ions traveling down the axon, which is further transmitted to other neurons through a junction known as the synapse. A single neuron can be connected to more than 10^4 neurons; the transmitting neuron is referred to as a presynaptic neuron and the receiving is termed a postsynaptic neuron.

The action potential consists of short electrical pulses, which has a shape of a narrow spike and travels down the axon, from soma to synapse. The shape of the action potential is similar among neurons, and it is therefore believed that the neural networks communicate through the frequency and timing of fired action potentials. Action potentials are regularly observed as chains of distinct signals, where a chain is known as a spike train. There is a minimal time frame between two action potentials, known as the absolute refractory period. This period is followed by relative refractoriness, referring to the time where it is possible, but difficult to fire a new action potential.

In the vertebrate brain the chemical synapses are the most common, where a complex chain of bio-chemical processes are triggered when receiving an action potential. This process leads to a release of neurotransmitter molecules from the presynaptic terminal into the synaptic cleft, which is a tiny gap between the pre– and postsynaptic neuron. Specialized receptors in the postsynaptic cell membrane detects the transmitter molecules and open membrane bound ion channels, transferring the ions from the extracellular medium into the postsynaptic neuron. The chemical signal is finally translated to an electrical response responsible for the postsynaptic potential processed in the soma. Synapses perform a temporal filtering of the action potential where the sharp spiky form of an action potential is translated to a wider round form observed in the postsynaptic potential.

The action potential and the postsynaptic potential are obtained by the potential difference between the outside and the inside of the neuron and are both forms of membrane potentials. If the postsynaptic change in the membrane potential due to an presynaptic action potential is negative (resp. positive) the presynaptic neuron is called inhibitory (resp. excitatory). A neuron can only be inhibitory or excitatory, this is commonly referred to as Dale's principle. The membrane acts as an insulator between the extracellular medium and the inside of the neuron. Both mediums are electrically conductive, giving rise to a capacitance with a membrane time constant denoted τ_m (Sterratt et al., 2011)[p. 33].

In a small portion of the mammalian brain, thousands of spikes are emitted each millisecond, referred to as population activity. It is commonly believed that the majority of information generated in a population can be obtained by its mean firing rate. The firing rate is defined by a temporal average of spikes, counted in a specific time window. Denote the number of spikes in a time window T as $N_{sp}(T)$. Then the firing rate v is defined as

$$v = \frac{N_{sp}(T)}{T}.$$

2.2 Derivation of the NFL model

We begin the derivation of a neural-field model by considering a microscopic network and work our way up the scales to a macroscopic field model. The following derivation of the scalar neural-field model is adapted from Gerstner and Kistler (2002)[ch. 6.5];Bressloff (2012)[sec. 2].

Let a network of neurons $i = 1, ..., N$ be synaptically connected as depicted in Fig. 1. Neuron j fires an action potential at times $\{T_j^l | l \in \mathbb{Z}\}$. A temporal filtering effect (see Fig. 1) in the synapse-dendrite process is defined as $\Phi_{ij}(t)$. Further assume that the synaptic inputs can be linearly summed. Then the total synaptic input to the soma $u_i(t)$ is given by

$$u_i(t) = \sum_{j=1}^{N} \sum_{l} \Phi_{ij}(t - T_j^l) = \sum_{j=1}^{N} \int_{-\infty}^{t} \Phi_{ij}(t-s) a_j(s) \, \mathrm{d}s. \tag{2.1}$$

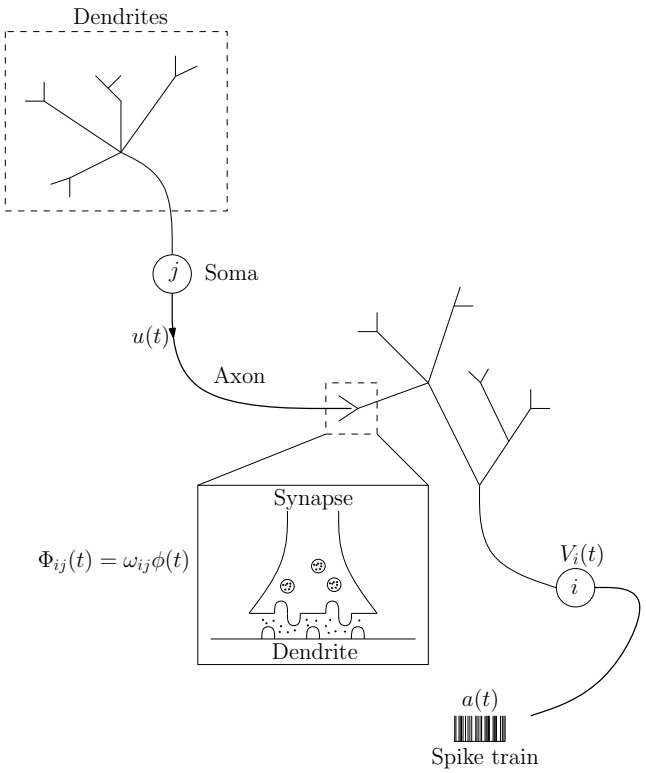

Figure 1: Illustration of synaptically connected neurons. The pre– and postsynaptic neuron is denoted i and j respectively. The axon of the presynaptic neuron is connected to the dendrite of the postsynaptic neuron through a synapse. The temporal filtering effect performed in the synapse-dendrite process is denoted $\Phi_{ij}(t)$. The synaptic input from j to i is denoted $u(t)$ causing change in the membrane potential denoted $V_i(t)$ due to action potentials. A chain of action potentials (spike train) is denoted $a(t)$.

Here the spike train $a_j(t)$ is given as

$$a_j(t) = \sum_l \delta(t - T_j^l),$$

where δ is the Dirac delta function. As depicted in Fig. 1, the membrane potential of the soma of neuron j is denoted V_j. Further, the firing times T_j^l is defined by the threshold condition given as

$$T_j^l = \inf \left\{ t, t > T_j^l \,\middle|\, V_j(t) > u_\theta, \frac{\mathrm{d}}{\mathrm{d}t} V_j(t) > 0 \right\},$$

where u_θ denote the threshold for firing an action potential.

External currents are assumed negligible. Thus V_j will depend on the electrical properties of the synapses (such as conductance) and the electrical activity of the coupled neurons. Assume that the change in synaptic input is lower than the change in membrane potential i.e. $\frac{\mathrm{d}u_j}{\mathrm{d}t} < \frac{\mathrm{d}V_i}{\mathrm{d}t} \, \forall t \in \mathbb{R}_0^+$. This will be a fact if the network is partitioned in a multiple of homogeneous networks firing asynchronous (Gerstner and Kistler, 2002)[ch. 6.4]. Asynchronous firing means that the spike trains from each neuron in a homogeneous population are uncorrelated (Bressloff, 2014)[p. 234]. Then we can assume that the population activity is equal to the mean firing rate of neuron i in this population. We may approximate the spike train $a_j(t)$ with an instantaneous firing rate $f_j(u_j(t))$. Here f_j is a firing-rate function giving the population-averaged firing rate of a local homogeneous population of neurons. Let two populations be given as P_n and P_m. Further, let neuron $i \in P_n$ and $j \in P_m$. Then, since the activity in P_n is the average activity of neuron i we let the indexes $i, j \to n, m$.

Let $\Phi_{nm}(t) = \omega_{nm}\phi(t)$, where ω_{nm} determines the synaptic coupling strength of population m to population n. $\phi(t)$ is called the response kernel, and it models the effect of spike emission and reception. Hence for Eq. (2.1) we get

$$u_n(t) = \sum_{m=1}^{N} \int_{-\infty}^{t} \omega_{nm}\phi(t-s) f_m(u_m(s)) \, \mathrm{d}s. \tag{2.2}$$

Here N is the number of neural populations considered.

Let a set of neurons from a cortical column be homogeneous and spread out on a one dimensional axis as shown in Fig. 2. That is, discretize the axis in segments of length d and let all the neurons of

population P_n be placed in the segment $[nd, (n+1)d]$. Let $\Phi_{nm}(t) = \rho d\Phi(nd, md, t)$ where ρ is the average spatial neuron density. The number of neurons in segment $[nd, (n+1)d]$ is $N_n = \rho d$, we may thus rewrite Eq. (2.2) as

$$u(nd,t) = \rho d \sum_{m=1}^{N} \int_{-\infty}^{t} \omega(nd, md)\phi(t-s) f(u(md,s))\,\mathrm{d}s. \tag{2.3}$$

Remark. We have specified that ρ denotes the *average* neuron density, this is not specified by Gerstner and Kistler (2002), neither do they specify that ρ varies.

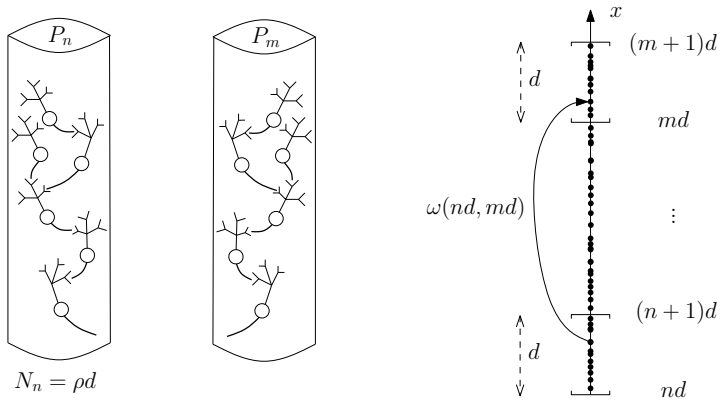

Figure 2: Illustration of a neural field on a one dimensional axis. The homogeneous neuron population P_n is put in the segment $[nd, (n+1)d]$ with length d. The coupling strength between two neuron populations $P_{m,n}$ is denoted $\omega(nd, md)$ and describes the average coupling strength between two points on the axis when $d \to 0$. The average density of neurons on the axis is denoted ρ and N_n denotes the number of neurons in population P_n.

Assume a bounded sum in the integrand of Eq. (2.3). Then we can interchange the sum and the integral, and by taking the limit $d \to 0$ we get

$$\lim_{d\to 0} u(nd,t) = \lim_{d\to 0} \int_{-\infty}^{t} \rho d \sum_{m=1}^{N} \omega(nd, md)\phi(t-s) f(u(md,s))\,\mathrm{d}s. \tag{2.4}$$

If the integrand in Eq. (2.4) is uniformly convergent we may interchange limit and integration. Then the sum will go to an integral and a neural-field model emerges in the form of a Volterra integral equation presented as

$$u(x,t) = \int_{-\infty}^{t} \int_{\Omega} \omega(x,x')\phi(t-s) f(u(x',s))\,\mathrm{d}x'\,\mathrm{d}s. \tag{2.5}$$

Here $u(x,t)$ denotes the average electrical activity of neuron populations at position x and time t, the spatial extent of the network is denoted Ω and the neuron density ρ is absorbed into $\omega(x,x')$. Note that for homogeneous and isotropic media, the coupling strength function ω is only dependent on the distance between neurons in position x and x', i.e. $\omega(x,x') = \omega(|x-x'|)$. Translational invariance ($\omega(x,x') = \omega(x-x')$) is obtained from homogeneity, and isotropy yield $\omega(z) = \omega(|z|)$ (Ermentrout, 1998)[p. 387]. The coupling strength between position x and x' gives the average coupling strength between two neuron populations separated by the distance $|x-x'|$.

Let the response kernel be given by $\phi(t) = \tau^{-1}\exp(-t/\tau)$ where τ is a decay time constant[1] of the synapses in a population of neurons. Then by the assumptions imposed in Appendix B.2 we take the temporal derivative of Eq. (2.5) and get the scalar neural-field model given as

$$\tau \frac{\partial}{\partial t} u(x,t) = -u(x,t) + \int_{\Omega} \omega(x,x') f(u(x',t))\,\mathrm{d}x'. \tag{2.6}$$

The time constant τ can trivially be scaled to one without loss of generality. Then by substituting the firing-rate function f by the sigmoidal function S_β, we get the NFL model (1.1). This substitution yields a statistical-mechanical approach and gives a mean field model, where the firing-rate function gives the probabilities for activity in a spatial area, and not the firing rate itself (Ermentrout, 1998)[p. 362].

[1] This time constant is related to the membrane time constant τ_m (Ermentrout, 1998)[p. 363]

2.3 PDE versus ODE formalism

The brain matter is static, meaning that the neurons or the populations of neurons do not change their spatial coordinates over time. From an experimental point of view, the spatial coordinates in the NFL model represent points of measuring the average neural activity. Imagine a spatially fixed needle, measuring only the temporal changes in the neural activity. A fixed x in Eq. (2.6) corresponds to a focus on a particular neural population. Thus, the biophysical background of the NFL model indicates that the spatial coordinate x can be regarded as a continuous parameter.

A discrete analog to Eq. (2.6) can be found in the integrate and fire network (IF) model. The IF model is obtained from Eq. (2.2) where we give the response kernel as $\phi(t) = \tau^{-1}\exp(-t/\tau)$. By further assuming a bounded sum we may interchange the sum and the integral. Then by performing a temporal differentiation on both sides we get

$$\tau\frac{\mathrm{d}}{\mathrm{d}t}u_n(t) = -u_n(t) + \sum_{m=1}^{N}\omega_{nm}f(u_m(t)), \quad n = 1, ..., N. \tag{2.7}$$

Here the sub-indexes m, n denote homogeneous neural populations as coupled N nonlinear first-order ODEs. Note the similarity of Eq. (2.7) and a spatially discretized version of Eq. (2.6), i.e. where the integral on the right hand side (r.h.s.) is discretized by e.g. the rectangular rule. In biophysical terms, the transition from Eq. (2.7) to Eq. (2.6) represents a transition from a finite to an infinite number of neurons (Gerstner and Kistler, 2002).

Equation (2.6) can be regarded as an extrapolation of Eq. (2.7); from a finite to an infinite dimensional system. Equation (2.6) further represents a continuum of nonlinear first-order ODEs parametrized by the spatial coordinates. Indicating that an extrapolation of finite dimensional theory from ODEs can be suitable for analyzing Eq. (2.6).

With regard to well-posedness, the existence theory from ODEs are well understood with the fundamental existence and uniqueness theorem, namely the Picard–Lindelöf theorem. In Section 3 we perform a well-posedness study of Eq. (1.1) adapted from Potthast and Beim Graben (2010). As argued by them, the local existence theorem given here is a type of the Picard–Lindelöf theorem.

A different method of analysis (see e.g. Ermentrout and McLeod (1993); Laing and Troy (2003); Coombes (2005)) is to re-cast the NFL model into an equivalent local form; a higher order nonlinear PDE. This method arose in an analysis of traveling wave solutions providing a co-moving frame of reference to the wave. This recasting is done by means of Fourier transforms and by exploiting a spatial convolution property of the integral in Eq. (2.6). Here the Fourier transform of the connectivity function ω is assumed to be a rational function of k^2, where k is the wave number of the Fourier transform. In detail, the Fourier transform $\mathtt{F}$ of ω is $\mathtt{F}(\omega) = Q(k^2)/P(k^2)$, $P(k^2) \neq 0$ where Q, P are polynomials in k^2 with $deg(P) \geq deg(Q) + 1$. These assumptions put a severe restriction on the choice of connectivity function, making the model less general. In addition, the PDE formalism obtained via this re-casting provides a complicated model. The well-posedness theory of higher order nonlinear PDEs can be very complicated compared to the well-posedness theory of ODEs.

From a numerical point of view, the discretization of Eq. (2.6) is a fairly simple task when x is considered as a continuous parameter. Then it is possible to fix x and employ numerical theory from ODEs. This approach is more general than a numerical evaluation of the PDE approach since the connectivity function can be chosen freely. Further, numerical theory for ODEs can provide a safer frame for the analyst as it is more developed than the numerical theory for PDEs. By the arguments presented in this subsection, the PDE formalism is omitted in this thesis.

Before we begin the numerical analysis we will review a proof of the well-posedness of the NFL model.

3 The well-posedness of the NFL model

We begin this section by listing the assumptions imposed on the initial condition, the connectivity kernel and the firing-rate function. We further proceed by reviewing a proof of the global existence and uniqueness of a solution to the NFL model adapted from Potthast and Beim Graben (2010). Finally we review a stability analysis adapted from Nielsen et al. (2013).

3.1 Assumptions

The initial condition

The initial condition is defined in a Banach space of bounded continuous functions i.e.

$$u(x,0) = u_0(x) \in C(\Omega)$$

The connectivity kernel

We impose the following assumptions on the family of synaptic connectivity kernels ω.

a) The connectivity kernels $\omega : \Omega \times \Omega \to \mathbb{R}$ are real valued, continuous and piecewise smooth.

b) The connectivity kernels $\{\omega_x\}_{x\in\Omega}$ constitute a 1–parameter family of functions, parametrized by $x \in \Omega :\ \omega_x(x') \equiv \omega(x,x')$, where $\omega_x : \Omega \to \mathbb{R}$, $x \in \Omega$

c) The norm of the connectivity kernels satisfy the uniform bound

$$||\omega||_1 \leq C_\omega$$

where

$$||\omega||_1 \equiv \max_{x\in\Omega} ||\omega(x,\cdot)||_{L_1(\Omega)} = \max_{x\in\Omega} \left(\int_\Omega |\omega(x,x')|\ \mathrm{d}x' \right).$$

d) The connectivity kernels obey the Lipschitz condition (see Appendix B.6)

$$||\omega(x,\cdot) - \omega(\widetilde{x},\cdot)||_{L_1(\Omega)} \leq c_\omega\, |x - \widetilde{x}|\,, \quad c_\omega > 0.$$

The firing-rate function

The firing-rate function S_β can be expressed in terms of a scaling function $S : S_\beta(u) = S(\beta u)$. Here S_β is a member of a 1–parameter family, parametrized by the steepness parameter β.

Furthermore, S has the following properties.

a) S is a monotonically increasing function.

b) $S : \mathbb{R} \to [0,1]$.

c) $S \in BC^1(\mathbb{R}) \cap BC^2(\mathbb{R})$, implying that

$$|S(u) - S(v)| \leq S'_{\max}\, |u - v|\,. \tag{3.1}$$

We further define the maximum values of the derivatives of S as

$$S'_{\max} = \max_{u\in\mathbb{R}} \left(\frac{\mathrm{d}}{\mathrm{d}u} S(u) \right), \quad S''_{\max} = \max_{u\in\mathbb{R}} \left(\frac{\mathrm{d}^2}{\mathrm{d}u^2} S(u) \right).$$

d) $\lim\limits_{u\to+\infty} S(u) = 1$, $\lim\limits_{u\to-\infty} S(u) = 0$, $S(0) = \frac{1}{2}$. Hence in the limit where $\beta \to \infty$, the firing-rate function becomes a Heaviside step function, i.e.

$$\lim_{\beta\to\infty} S(\beta(u - u_\theta)) = H(u) = \begin{cases} 1, & u > u_\theta \\ \frac{1}{2}, & u = u_\theta \\ 0, & u < u_\theta \end{cases}.$$

e) The firing threshold is $0 < u_\theta < 1$.

f) The steepness parameter is nonzero and nonnegative ($\beta > 0$).

3.2 Volterra formulation

To prove existence and uniqueness of the Cauchy formulated NFL model (1.1), we convert the model to a Volterra fix point problem defined on an appropriate Banach space. Then we prove existence and uniqueness of the Volterra formulation by means of Banachs fixed point theorem. We further prove the equivalence between the Volterra formulation and the Cauchy formulation. Then any solution of the Volterra formulation is also a solution of the Cauchy formulated NFL model.

We begin by defining some appropriate spaces.

Definition 3.1. *For $t \in [0,T]$, where $T > 0$ and $x \in \Omega$ we define the Banach space $(X_T, ||\cdot||_T)$ as*

$$X_T \equiv BC(\Omega \times [0,T])$$

equipped with the norm

$$||u||_T \equiv \max_{x\in\Omega,\, t\in[0,T]} |u(x,t)|\,.$$

For $t \in [0,\infty)$, and $x \in \Omega$ we define the Banach space $(X_T, ||\cdot||_\infty)$ as

$$X \equiv BC(\Omega \times \mathbb{R}_0^+)$$

equipped with the norm

$$||u||_\infty \equiv \sup_{x\in\Omega,\, t\in\mathbb{R}_0^+} |u(x,t)|\,.$$

Definition 3.2. *The operators J, F and A are defined as*

$$J[u](x,t) \equiv \int_\Omega \omega(x,x')S(\beta(u(x',t)-u_\theta))\,\mathrm{d}x', \quad x \in \Omega,\, t \geq 0. \tag{3.2}$$

$$F[u](x,t) \equiv -u(x,t) + \int_\Omega \omega(x,x')S(\beta(u(x',t)-u_\theta))\,\mathrm{d}x', \quad x \in \Omega,\, t \geq 0. \tag{3.3}$$

$$A[u](x,t) \equiv u_0(x) + \int_0^t F[u](x,s)\,\mathrm{d}s, \quad x \in \Omega,\, t \geq 0. \tag{3.4}$$

Local existence and uniqueness is proved by the contraction mapping theorem; see Appendix B.1 i.e. that the fixed point problem $u(x,t) = A[u](x,t)$ has a unique solution $u^* \in X_T$ given as

$$u^*(x,t) = A[u^*](x,t). \tag{3.5}$$

To this end, we will first prove that the operator A is a contraction of $(X_T, ||\cdot||_T)$ i.e.

$$A : X_T \mapsto X_T$$

$$||A[u] - A[v]||_T \leq K\,|u-v|\,,\ 0 < K < 1\ \forall\, u, v \in X_T.$$

Since the NFL model does not depend explicitly on time we can employ the local arguments on an arbitrary time interval $[t_0, t_0+T]$ (Potthast and Beim Graben, 2010). Thus we can iterate the local existence and uniqueness results, giving global existence and uniqueness.

Theorem 3.1. *Assume that $u \in BC(\Omega \times [0,T])$. Then*

$$v = A[u] \in BC(\Omega \times [0,T]), \quad T > 0,$$

with A defined in Eq. (3.4), i.e. A is a mapping of X_T into X_T.

Proof. We begin by splitting the operator A in two parts such that $A = A_1 + A_2$ where

$$\begin{aligned} A_1[u](x,t) &\equiv u_0(x) - \int_0^t u(x,s)\,\mathrm{d}s, \\ A_2[u](x,t) &\equiv \int_0^t \int_\Omega \omega(x,x')S(v(x',s))\,\mathrm{d}x'\,\mathrm{d}s, \quad v(x,t) = \beta(u(x,t) - u_\theta). \end{aligned} \tag{3.6}$$

Continuity of A implies that

$$\lim_{h,k\to 0} [A[u](x+h,t+k) - A[u](x,t)] = 0. \tag{3.7}$$

For A_1 we derive the following chain of inequalities

$$\begin{aligned} &\left| \int_0^{t+k} u(x+h,s)\,\mathrm{d}s - \int_0^t u(x,s)\,\mathrm{d}s \right| \\ &\qquad = \left| \int_0^{t+k} u(x+h,s) - u(x,s)\,\mathrm{d}s + \int_t^{t+k} u(x,s)\,\mathrm{d}s \right| \\ &\qquad \le \int_0^{t+k} |u(x+h,s) - u(x,s)|\,\mathrm{d}s + \int_t^{t+k} |u(x,s)|\,\mathrm{d}s \\ &\qquad \le \max_{0<t<T} |u(x+h,t) - u(x,t)|\,T + |u(x,t+u_\theta k)|\,k, \quad 0 < u_\theta < 1. \end{aligned} \tag{3.8}$$

Here we tacitly used the mean value theorem for integrals to estimate the integral $\int_t^{t+k} |u(x,s)|\,\mathrm{d}s$; see Theorem B.3. From the inequalities in Eq. (3.8) and the continuity assumption on the initial condition u_0, we see that

$$\begin{aligned} &|A_1[u](x+h,t+k) - A_1[u](x,t)| \le \\ &|u_0(x+h) - u_0(x)| - \max_{0<t<T} |u(x+h,t) - u(x,t)|\,T + |u(x,t+u_\theta k)|\,k. \end{aligned} \tag{3.9}$$

Consequently the difference in Eq. (3.9) will be squeezed between zero and a bound approaching zero as $(h,k) \to (0,0)$.

We proceed by considering the non-linear operator A_2, and derive the following chain of inequalities

$$\begin{aligned} &|A_2[u](x+h,t+k) - A_2[u](x,t)| \\ &= \left| \int_0^{t+k} \int_\Omega \omega(x+h,x')S(v(x',s))\,\mathrm{d}x'\,\mathrm{d}s - \int_0^t \int_\Omega \omega(x,x')S(v(x',s))\,\mathrm{d}x'\,\mathrm{d}s \right| \\ &= \left| \int_0^{t+k} \int_\Omega [\omega(x+h,x') - \omega(x,x')]S(v(x',s))\,\mathrm{d}x'\,\mathrm{d}s + \int_t^{t+k} \int_\Omega \omega(x,x')S(v(x',s))\,\mathrm{d}x'\,\mathrm{d}s \right| \\ &\le \int_0^{t+k} \int_\Omega |\omega(x+h,x') - \omega(x,x')|\,\mathrm{d}x'\,\mathrm{d}s + \int_t^{t+k} \int_\Omega |\omega(x,x')|\,\mathrm{d}x'\,\mathrm{d}s \\ &\le c_\omega\,|h|\,m(\Omega) \int_0^{t+k} \mathrm{d}s + C_\omega k. \end{aligned} \tag{3.10}$$

Here we have denoted $v(x,t) = \beta(u(x,t) - u_\theta)$, and used assumption b) on the firing rate function S and d) on the connectivity function ω; see Section 3.1. In the limit where $(h,k) \to (0,0)$ the estimate

in Eq. (3.10) is squeezed between zero and a bound approaching zero. We further see that Eq. (3.7) satisfies

$$\lim_{h,k\to 0}\left[(A_1+A_2)[u](x+h,t+k)-(A_1+A_2)[u](x,t)\right]=0.$$

Further, the operator A satisfies the uniform bound on X_T given as

$$\begin{aligned}|A[u](x,t)| &\leq |u_0| + \int_0^t |u(x,s)|\,\mathrm{d}s + \int_0^t\int_\Omega |\omega(x,x'|\,\mathrm{d}x'\,\mathrm{d}s\\ &\leq ||u_0||_T + ||u||_T\,T + C_\omega T.\end{aligned}$$

Here we have exploited assumption c) imposed on the connectivity kernel and assumption b) on the firing-rate function; see Section 3.1.

The boundedness and continuity combined is a proof of the fact that A maps X_T into itself (Sobolev). □

Theorem 3.2. *Assume that the initial condition, the connectivity kernel and the firing-rate function satisfy the assumptions listed in Section 3.1. Further assume that*

$$T<\frac{1}{1+\beta S_{\max}^{'}C_\omega}.$$

Then $A: X_T \mapsto X_T$ defined in Eq. (3.4) *is a contraction mapping of X_T i.e.*

$$||A[u]-A[v]||_T \leq K\,||u-v||_T\,,\ K<1\ \forall\, u,v\in X_T.$$

Consequently, the fixed point problem (3.5) *has a unique solution on $\Omega\times[0,T]$.*

Proof. We split the operator A in two parts $A=A_1+A_2$ (see Theorem 3.1) with A_1, A_2 defined in Eq. (3.6). Then one can immediately see that A_1 satisfies the following inequality given as

$$||A_1[u]-A_1[v]||_T \leq T\,||u-v||_T\,,\ \forall\, u,v\in X_T.$$

To evaluate the absolute difference $|A_2[u]-A_2[v]|$ we derive the following chain of inequalities of the absolute difference of the integral operator J defined in Eq. (3.2).

$$\begin{aligned}|J[u](x,t)-J[v](x,t)| &\leq \int_\Omega |\omega(x,x')|\,|S(\beta(u(x',t)-u_\theta))-S(\beta(v(x',t)-u_\theta))|\,\mathrm{d}x'\\ &\leq \beta S_{\max}^{'}\int_\Omega |\omega(x,x')|\,|u(x',t)-v(x',t)|\,\mathrm{d}x'\\ &\leq \beta S_{\max}^{'}C_\omega\,||u-v||_T\,.\end{aligned}\tag{3.11}$$

Here we have exploited the fact that the firing-rate function is Lipschitz continuous with the Lipschitz constant defined in Eq. (3.1). Integration from 0 to t on both sides of Eq. (3.11) yields

$$||A_2[u]-A_2[v]||_T \leq T\beta S_{\max}^{'}C_\omega\,||u-v||_T\,,\ \forall\, u,v\in X_T.$$

Hence

$$||A[u]-A[v]||_T \leq K\,||u-v||_T\,,\ \forall\, u,v\in X_T,$$

where

$$K=(1+\beta S_{\max}^{'}C_\omega)T.$$

Since $T<\frac{1}{1+\beta S_{\max}^{'}C_\omega}$, we have $K<1$ from which it follows that $A: X_T\mapsto X_T$ is a contraction of X_T.

Remark. $K<1 \iff T<\frac{1}{1+\beta S_{\max}^{'}C_\omega}$ implies that if β have large values, then T has to be very small.

By the contraction mapping theorem (Appendix B.1) there exists a unique solution u^* to the equation

$$u^*(x,t) = A[u^*](x,t).$$

□

A uniform bound of the solution to the NFL model is proved in the following lemma. This result is then used in Theorem 3.3 where we prove global existence and uniqueness.

Lemma 3.1. *The solution u of the NFL model* (1.1)*, with an initial condition u_0, connectivity kernel ω and a firing-rate function S satisfying the assumptions listed in Section 3.1 is uniformly bounded by C_{tot}, where*

$$C_{tot} \equiv \max(||u_0||_\infty, C_\omega).$$

Proof. Consider the rearranged NFL model with $v(x,t) = \beta(u(x,t) - u_\theta)$

$$\frac{\partial u(x,t)}{\partial t} + u(x,t) = \int_\Omega \omega(x,x')S(v(x',t))\,\mathrm{d}x'.$$

By the use of an integrating factor we obtain

$$\frac{\partial}{\partial t}(u(x,t)\mathrm{e}^t) = \mathrm{e}^t \int_\Omega \omega(x,x')S(v(x',t))\,\mathrm{d}x'.$$

Integrate on both sides from 0 to t:

$$u(x,t)\mathrm{e}^t - u_0(x) = \int_0^t \mathrm{e}^s \int_\Omega \omega(x,x')S(v(x',t))\,\mathrm{d}x'\,\mathrm{d}s.$$

Then by rearranging, the potential u is given as

$$u(x,t) = u_0(x)\mathrm{e}^{-t} + \int_0^t \mathrm{e}^{-(t-s)} \int_\Omega \omega(x,x')S(v(x',t))\,\mathrm{d}x'\,\mathrm{d}s.$$

Finally, we derive the following chain of inequalities

$$\begin{aligned}
|u(x,t)| &\le |u_0(x)|\,\mathrm{e}^{-t} + \int_0^t \left|\mathrm{e}^{-(t-s)}\right| \int_\Omega |\omega(x,x')|\,|S(v(x',t))|\,\mathrm{d}x'\,\mathrm{d}s \\
&\le |u_0(x)|\,\mathrm{e}^{-t} + \int_0^t \left|\mathrm{e}^{-(t-s)}\right| \int_\Omega |\omega(x,x')|\,\mathrm{d}x'\,\mathrm{d}s \\
&\le |u_0(x)|\,\mathrm{e}^{-t} + \int_0^t \left|\mathrm{e}^{-(t-s)}\right| ||\omega||_1\,\mathrm{d}s \\
&\le ||u_0||_\infty\,\mathrm{e}^{-t} + \left|1 - \mathrm{e}^{-t}\right| C_\omega \\
&\le (||u_0||_\infty - C_\omega)\mathrm{e}^{-t} + C_\omega \\
&\le C_{tot}.
\end{aligned}$$

Here we tacitly used the triangle inequality, assumption b) on the firing rate function S, and assumption c) on the connectivity kernel; see Section 3.1. □

Theorem 3.3. *Let the initial condition, connectivity kernel and the firing-rate function satisfy the assumptions listed in Section 3.1. Then the fixed point problem* (3.5) *has a unique solution on $\Omega \times \mathbb{R}_0^+$.*

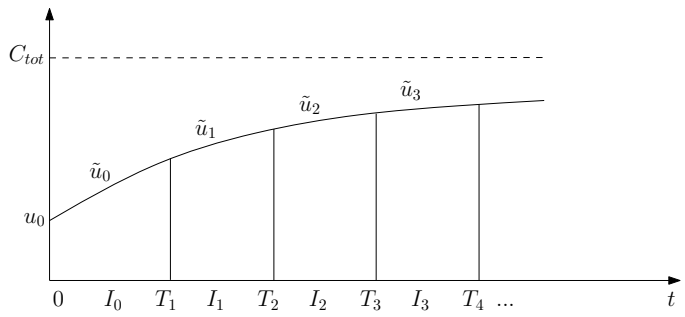

Figure 3: A sketch of the global existence and uniqueness proof. The solution $u = \widetilde{u}_n$, $u \in I_n$, $n = 0, 1, 2, ...$ of the NFL model is represented by the solid curved line, and is uniformly bounded by C_{tot} represented by the dashed line. The local existence and uniqueness of the NFL model is iterated over the temporal intervals $I_n = [T_n, T_{n+1}]$, $n = 0, 1, 2, ...$ where $T_0 = 0$.

Proof. The proof is carried out in an iterative way, graphically illustrated in Fig. 3.

From Theorem 3.2 we know that the solution of the Volterra formulation exists and is unique on the space $\Omega \times I_0$ where $I_0 = [0, T_1]$. By Lemma 3.1 we know that the solution $\widetilde{u}_0$ do not blow up on the interval I_0. In addition, the temporal derivative is defined and continuous in the end point T_1. Thus, we introduce

$$\widetilde{u}_1(x, T_1) = \lim_{t \to T_1^-} \widetilde{u}_0(x, t) < \infty. \tag{3.12}$$

and

$$J[\widetilde{u}_1](x, T_1) = \lim_{t \to T_1^-} J[\widetilde{u}_0](x, t) \tag{3.13}$$

Hence, we can define a new initial condition starting at the endpoint of I_0 by Eq. (3.12). We further define a new interval $I_1 = [T_1, T_2]$. Then the solution $\widetilde{u}_1$ exists and is unique on $\Omega \times I_1$ by Theorem 3.2 with

$$T_2 < \frac{1}{1 + \beta S'_{\max} C_\omega} + T_1 < \frac{2}{1 + \beta S'_{\max} C_\omega}.$$

From Lemma 3.1 and Eq. (3.13) we know that $\widetilde{u}_1 \in BC^1(\Omega \times I_1)$ and we can thus continue in an iterative way by defining a new interval $I_2 = [T_2, T_3]$. Further, from Theorem 3.2 we know that the solution of the Volterra formulation exists and is unique on the space $\Omega \times I_n$ i.e.

$$\widetilde{u}_n(x, t) = A[\widetilde{u}_n](x, t).$$

Let $I_n = [T_{n-1}, T_n]$, $u = \widetilde{u}_n$, $u \in I_n$, $n = 1, 2, ...$ and $T_0 = 0$. We further see from Theorem 3.2 that $K_{n-1} = (1 + \beta S'_{\max} C_\omega)(T_n - T_{n-1}) < 1, \quad n = 1, 2, ...$ Thus we get

$$\begin{aligned} T_1 &< \frac{1}{1 + \beta S'_{\max} C_\omega} \\ T_2 &< \frac{1}{1 + \beta S'_{\max} C_\omega} + T_1 < \frac{2}{1 + \beta S'_{\max} C_\omega} \\ &\vdots \\ T_n &< \frac{1}{1 + \beta S'_{\max} C_\omega} + T_{n-1} < \frac{n}{1 + \beta S'_{\max} C_\omega}, \quad n = 1, 2, ... \end{aligned}$$

The initial conditions in each point T_n, $n > 0$ are defined as

$$\widetilde{u}_n(x, T_n) = \lim_{t \to T_n^-} \widetilde{u}_n(x, t) < \infty,$$

and the temporal derivative is defined and continuous in the end points T_n.

The union of the intervals $I_1, I_2, ..., I_\infty$ is $\cup_{i=0}^{\infty} I_i = \mathbb{R}_0^+$, thus a solution to the Volterra formulation exists and is unique globally. □

The Volterra formulation can contain a larger class of solutions than that of the Cauchy formulation. Hence we have to ensure that any solution to the Cauchy formulation given in Eq. (1.1) is a solution to the Volterra formulation given in Eq. (3.5) and vice versa. The next theorem proves equivalence between the Volterra formulation and the Cauchy formulation.

Theorem 3.4. *A solution on $\Omega \times [0,T]$ of the fixed point problem* (3.5) *with A defined in Eq.* (3.4) *exists and is unique if and only if a solution of the Cauchy formulation* (1.1) *exists and is unique i.e.*

$$u = A[u] \iff \frac{\partial u}{\partial t} = F[u],\ u|_{t=0} = u_0$$

Proof. By assumption we know that $u(x,\cdot) \in C^1(\mathbb{R}_0^+)$ allowing the fundamental theorem of calculus to be employed on the Cauchy formulation, thus deriving the Volterra formulation. The initial conditions are equivalent, which is demonstrated by $u|_{t=0} = A[u]|_{t=0} = u_0$. Further, let the mapping $\zeta_x : [0,T] \mapsto \mathbb{R}$ be be defined as

$$\zeta_x(t) \equiv F[u](x,t),$$

which is continuous w.r.t the temporal variable t where x is considered a fixed parameter. The solution to $u(x,t) = A[u](x,t)$ with A defined in Eq. (3.4) is thus continuously differentiable with respect to $t \geq 0$ and the derivative is continuous in $\mathbb{R}_0^+$ (Potthast and Beim Graben, 2010). □

We have demonstrated that the NFL model is globally well posed in the sense that there exists a unique solution for all $x \in \Omega$ and $t > 0$. The next section will regard stability, and we finally state global well posedness in the sense of Hadamard. His requirements is in addition to global existence and uniqueness, a continuous mapping from initial conditions to solution.

3.3 Stability

For the sake of completeness we present one stability result of particular interest from Nielsen et al. (2013).

Let u and $\widetilde{u}$ be two solutions of the Cauchy formulation (1.1) with corresponding initial conditions and steepness parameters $u_0, \widetilde{u}_0, \beta, \widetilde{\beta}$. Then for $u_0 = \widetilde{u}_0$, $t \in [0,T]$ and the norm $||\cdot|| \equiv \max_{x\in\Omega} |\cdot|$ one get the equality

$$||u - \widetilde{u}||(T) = S'_{\max} C_\omega T (C_{tot} + u_\theta) \left|\beta - \widetilde{\beta}\right| + (1 + \widetilde{\beta} S'_{\max} C_\omega) \int_0^T ||u - \widetilde{u}||(t)\, \mathrm{d}t.$$

Since $g(t) = ||u - \widetilde{u}||(t)$ satisfies the condition of the Grönwall inequality and a solution of Eq. (1.1) is uniformly bounded, one get the stability estimate

$$||u - \widetilde{u}||(T) \leq S'_{\max} C_\omega T (C_{tot} + u_\theta) \left|\beta - \widetilde{\beta}\right| \cdot \exp\left((1 + \widetilde{\beta} S'_{\max} C_\omega) T\right). \tag{3.14}$$

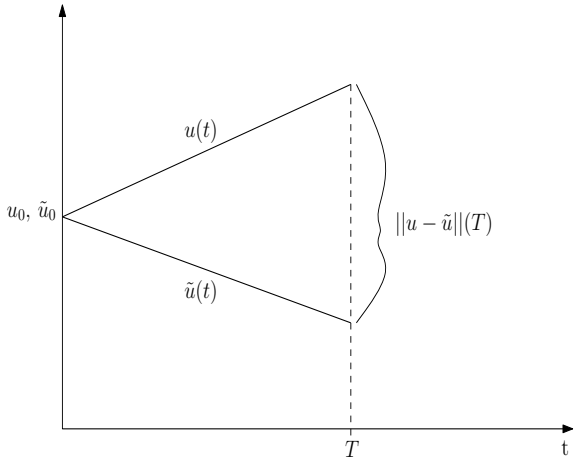

Figure 4: The separation distance $||u - \widetilde{u}||(T)$ at time T of two solutions of the NFL model initiated with equal initial conditions u_0 and $\widetilde{u}_0$. The separation distance is due to a perturbation on the steepness parameter $\widetilde{\beta}$. If $u(T) \to \widetilde{u}(T)$, $\beta \to \widetilde{\beta}$, then a solution is continuous dependent on the steepness parameter.

Since $||u - \widetilde{u}||(T) \to 0$, $\beta \to \widetilde{\beta}$ the mapping $Q : \beta \to u(\cdot, t)$ is continuous. The proof of a continuous mapping from initial conditions to solutions is omitted in this thesis, but is proven in Nielsen et al. (2013) with a similar argument as that of Eq. (3.14), thus ensuring global well-posedness in the sense of Hadamard.

In Eq. (3.14), $\widetilde{\beta}$ is in the argument of the exponential function. Therefore, this estimate can not guarantee that u and $\widetilde{u}$ remain close for even small perturbations of β. Hence, as argued by Nielsen et al. (2013) the model (1.1) is only 'theoretically' stable and some serious issues can occur in simulations due to finite precision of computers. This issue is analyzed more closely in the the next sections.

4 Numerical analysis

This section will mainly focus on the forward Euler and Heun's RK2 (from hereby only referred to as RK2) method employed on the NFL model in order to get a better understanding of some of the numerical properties of the NFL model. For the forward Euler method we derive the truncation error and the numerical error with respective upper bounds. We further derive the RK2 method and an upper bound of its truncation error. In order to assess efficiency of the forward Euler and RK2 method, the upper bounds of the respective truncation errors are finally compared.

We introduce the section by a simple example of a general non linear autonomous ODE and give definitions from numerical error-theory.

4.1 Definitions

Let a general nonlinear autonomous ODE be given as

$$\frac{\mathrm{d}\widetilde{u}}{\mathrm{d}t}(t) = f(\widetilde{u}(t)), \quad \widetilde{u}(0) = u_0,$$

where $\widetilde{u} \in C^1(\mathbb{R}_0^+)$. To approximate $\widetilde{u}(t)$ one can discretize the time variable through the points $t_n = \Delta t n$ and set up a new set of equations which can be solved on a computer. A typical example is the explicit[2] one-step method given as

$$u^{n+1} = F(u^n; \Delta t), \quad u^0 = u_0, \tag{4.1}$$

where u^n approximates $\widetilde{u}(t_n)$. The error obtained when Eq. (4.1) is employed on $\widetilde{u}$ is commonly referred to as the truncation error, defined as

$$R^n = \widetilde{u}^{n+1} - F(\widetilde{u}^n; \Delta t).$$

The truncation error is also known as the local (truncation) error, meaning error obtained by doing one step in the numerical method. If the truncation error is $\mathcal{O}(\Delta t^{p+1})$ where Δt is the discretization stepping length, then the method is of order p.

If the truncation error satisfies the limit

$$\lim_{\Delta t \to 0} \frac{R^n}{\Delta t} = 0,$$

then the numerical method is consistent, i.e. all methods of order greater than one ($p \geq 1$) are consistent (Darmofal, 2005).

If the maximal numerical error i.e. $\max_{0 \leq t_n \leq T} |u - \widetilde{u}| = 0$, $\Delta t \to 0$, then u converges to $\widetilde{u}$ and the numerical method is convergent. Further, if the maximal numerical error satisfies $\max_{0 \leq t_n \leq T} |u - \widetilde{u}| \leq C\Delta t^r$, then r is defined as the rate of convergence. For a order p method it is expected that $r = p$ (Darmofal, 2005).

Stability testing of a numerical method is traditionally performed by observing the evolution of numerical errors when the method is applied on a given test problem. If an error introduced at some stage of the calculation do not 'blow up' as one steps through the discretized region, then the method is said to be zero-stable. The Dahlquist equivalence theorem states that consistent and zero-stable methods are convergent, however, the converse is not necessarily true.

Test problems normally give stability regions in the complex plane, and if this region contains the left half of the complex plane, then the method is said to be A-stable. A-stable methods are more likely to produce stable approximations of stiff problems without significantly reduced stepping lengths. An ODE is said to be stiff if it requires a significant reduction of the stepping length when approximated in the whole, or in parts of its domain of definition (Iserles, 2009). Explicit methods are generally not A-stable, and instabilities are likely to occur if the temporal stepping length is not carefully selected when explicit methods are applied to stiff problems. There are no precise definitions of stiffness and in some cases, identifying stiffness can rely on observing instable behavior during approximations.

The often simple test problems only guarantee a stable method for a certain class of problems. Numerical stability of a given problem can be highly individual and it can be a major task to investigate and fully understand its numerical stability properties. Therefore, we will analyze the NFL model when

[2] In contrast to an implicit method given as $G(u^{n+1} - F(u^n; \Delta t)) = 0, \quad u^0 = u_0$

it is approximated by the simple forward Euler method. Stiffness of the NFL model is indicated if the method requires a significant reduction of Δt in some, or in the whole part of its domain of definition.

The truncation error gives the error of one 'step' in the discretized region and can give a good indication of how a numerical method will perform. Therefore, we derive and analyze only the truncation error of the RK2 method.

4.2 Preliminary analysis

The numerical analysis of the forward Euler and the RK2 method require several bounds in order to assess convergence[3] and consistency. For the forward Euler and RK2 method we need bounds of the second– and third-order temporal derivatives of the NFL model. The last bound considered is of the difference $|F[u] - F[v]|$ which is later used to derive a bound of the numerical error in the forward Euler method.

To prove bounds on the second– and third-order temporal derivative, we introduce a bound of the operator F.

Lemma 4.1. *The operator $F[u](x,t)$ is bounded by $C_\omega + C_{tot}$.*

Proof. Let $v(x,t) = \beta(u(x,t) - u_\theta)$. Then we readily obtain

$$\begin{aligned}
|F[u](x,t)| &= \left| -u(x,t) + \int_\Omega \omega(x,x') S(v(x',t))\,\mathrm{d}x' \right| \\
&\leq |u(x,t)| + \int_\Omega |\omega(x,x')|\,|S(v(x',t))|\,dx' \\
&\leq |u(x,t)| + \int_\Omega |\omega(x,x')|\,dx' \\
&\leq |u(x,t)| + ||\omega||_1 \\
&\leq C_{tot} + C_\omega.
\end{aligned}$$

□

Lemma 4.2. *The second– and third-order temporal derivative of the NFL model is bounded. The bounds are given as*

$$\left| \frac{\partial^2}{\partial t^2} [u(x,t)] \right| \leq (C_{tot} + C_\omega)(1 + \beta S'_{\max} C_\omega),$$

and

$$\left| \frac{\partial^3}{\partial t^3} [u(x,t)] \right| \leq (C_\omega + C_{tot}) \left(\left(1 + \beta C_\omega S'_{\max}\right)^2 + \beta^2 C_\omega S''_{\max} (C_\omega + C_{tot}) \right).$$

Proof. Let $v(x,t) = \beta(u(x,t) - u_\theta)$. Then the second-order temporal derivative of the solution u of the NFL model is presented as

$$\begin{aligned}
\frac{\partial^2}{\partial t^2} [u(x,t)] &= \frac{\partial}{\partial t} [F[u](x,t)] \\
&= -\frac{\partial u(x,t)}{\partial t} + \int_\Omega \omega(x,x') \frac{\partial}{\partial t} [S(v(x',t))]\,\mathrm{d}x' \\
&= -F[u](x,t) + \beta \int_\Omega \omega(x,x') \frac{\mathrm{d}}{\mathrm{d}v} [S(v(x',t))] \frac{\partial}{\partial t} [u(x',t)]\,\mathrm{d}x' \\
&= -F[u](x,t) + \beta \int_\Omega \omega(x,x') \frac{\mathrm{d}}{\mathrm{d}v} [S(v(x',t))]\, F[u](x',t)\,\mathrm{d}x'.
\end{aligned}$$

[3] We only prove convergence of the forward Euler method.

Thus we get the following chain of inequalities

$$\begin{aligned}\left|\frac{\partial^2}{\partial t^2}\left[u(x,t)\right]\right| &\leq |F[u](x,t)| + \left|\beta \int_\Omega \omega(x,x') \frac{\mathrm{d}}{\mathrm{d}v}\left[S(v(x',t))\right] F[u](x',t)\,\mathrm{d}x'\right| \\ &\leq |F[u](x,t)| + (C_{tot}+C_\omega)\beta \int_\Omega |\omega(x,x')| \left|\frac{\mathrm{d}}{\mathrm{d}v}\left[S(v(x',t))\right]\right| \mathrm{d}x' \\ &\leq (C_{tot}+C_\omega)(1+\beta S^{'}_{\max}\left|\left|\omega\right|\right|_1) \\ &\leq (C_{tot}+C_\omega)(1+\beta S^{'}_{\max} C_\omega).\end{aligned}$$

For the third-order temporal derivative we get

$$\begin{aligned}&\left|\frac{\partial^3}{\partial t^3}\left[u(x,t)\right]\right| = \left|\frac{\partial}{\partial t}\left(-F[u](x,t) + \beta \int_\Omega \omega(x,x') \frac{\mathrm{d}}{\mathrm{d}v}\left[S(v(x',t))\right] F[u](x',t)\,\mathrm{d}x'\right)\right| \\ &= \Bigg| -\frac{\partial}{\partial t}\left[F[u](x,t)\right] \\ &\qquad + \beta \int_\Omega \omega(x,x') \left(F[u](x',t)\frac{\partial}{\partial t}\left[\frac{\mathrm{d}}{\mathrm{d}v}\left[S(v(x',t))\right]\right] + \frac{\mathrm{d}}{\mathrm{d}v}\left[S(v(x',t))\right]\frac{\partial}{\partial t}\left[F[u](x',t)\right]\right)\mathrm{d}x'\Bigg| \\ &\leq \left|\frac{\partial}{\partial t}\left[F[u](x,t)\right]\right| + \beta C_\omega \int_\Omega \left|F[u](x',t)\beta \frac{\partial u}{\partial t}\frac{\mathrm{d}^2}{\mathrm{d}v^2}\left[S(v(x',t))\right]\right| + \left|\frac{\mathrm{d}}{\mathrm{d}v}\left[S(v(x',t))\right]\frac{\partial}{\partial t}\left[F[u](x',t)\right]\right| \mathrm{d}x' \\ &\leq (C_{tot}+C_\omega)(1+\beta S^{'}_{\max} C_\omega) + \beta C_\omega \left(\beta (C_{tot}+C_\omega)^2 S^{''}_{\max} + S^{'}_{\max}(C_{tot}+C_\omega)(1+\beta S^{'}_{\max} C_\omega)\right) \\ &= (C_\omega + C_{tot})\left(\left(1+\beta C_\omega S^{'}_{\max}\right)^2 + \beta^2 C_\omega S^{''}_{\max}\left(C_\omega + C_{tot}\right)\right)\end{aligned}$$

□

Lemma 4.3. *The norm of the difference between the operator F evaluated on two different functions $u, v \in X$ is bounded.*

Proof. By the triangle inequality and the Lipschitz continuity of the firing-rate function S we get

$$\begin{aligned}|F[u](x,t) - F[v](x,t)| &\leq |u(x,t)-v(x,t)| + \\ &\qquad \int_\Omega |\omega(x,x')|\,|S(\beta(u(x',t)-u_\theta)) - S(\beta(v(x',t)-u_\theta))|\,\mathrm{d}x' \\ &\leq \left|\left|u-v\right|\right|_\infty + \left|\left|\omega\right|\right|_1 \beta S^{'}_{\max}\left|\left|u-v\right|\right|_\infty \\ &\leq \left|\left|u-v\right|\right|_\infty (1+\beta S^{'}_{\max} C_\omega).\end{aligned}$$

□

We also require an appropriate space to be used in the discrete case where the spatial variable x is considered to be a continuous parameter and the temporal variable t is discretized. By the discretization we only sample temporal values at discrete points $t_n, n = 0, ..., N_t$ where N_t is the number of points considered. The solution of the NFL model evaluated at the discrete point t_n is denoted $u(x,t_n) = u^n(x)$.

Definition 4.1. *We define the Banach space $(X_D, ||\cdot||^D_\infty)$ as*

$$X_D \equiv BD(\Omega)$$

equipped with the norm

$$||u^n||^D_\infty \equiv \max_{x\in\Omega} |u^n(x)|\,.$$

The space X_D is graphically illustrated in Fig. 5, showing a discrete set of continuous, closed intervals. Since the NFL model has a separated dependence on the spatial and temporal variable, it can be treated as a continuum of ODEs; see Section 2.3. This fact is exploited in the following numerical analysis.

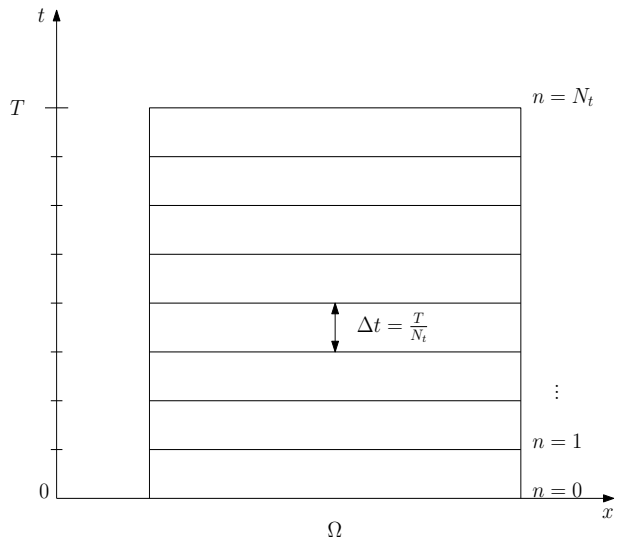

Figure 5: Illustration of the space X_D, discretized in the temporal direction giving a discrete set of continuous closed intervals. The temporal stepping length is denoted Δt, $T = N_t \Delta t$ expresses the stopping time, N_t represents the number of discretized points and Ω denotes the spatial domain.

4.3 Forward Euler approximation

Let the temporal variable t be discretized by t_n, $n = 0, 1, 2, ..., N_t$ as illustrated in Fig. 5. Denote the approximated solution of the NFL model as $u^n(x)$ evaluated at time t_n in the spatial point x. Note that the spatial variable x is considered a parameter which is always fixed when changing the temporal variable t. The forward Euler approximation of the temporal derivative is thus given as

$$\frac{\partial u}{\partial t} \approx \frac{u^{n+1}(x) - u^n(x)}{\Delta t}.$$

The NFL model can thus be approximated by the following explicit method

$$u^{n+1}(x) = u^n(x) + \Delta t F[u^n](x). \tag{4.2}$$

4.3.1 Consistency

The truncation error R^n is found as the remainder in Taylor's theorem. Here we formulate Taylors theorem in a special version (see Appendix B.5 for the normal version). Let $u(x,t)$ be continuously differentiable k times on the closed interval $\hat{I} = [t_n, t_n + \Delta t]$ and differentiable $k+1$ times in the open interval $I = (t_n, t_n + \Delta t)$. Also, let $\frac{\partial}{\partial t}u(x,t), ..., \frac{\partial^k}{\partial t^k}u(x,t)$ exist and be continuous at $t = t_n$. Then there exist a constant t_* between t_n and $t_n + \Delta t$ such that

$$u^{n+1}(x) = \sum_{i=0}^{k} \frac{1}{i!}\frac{\mathrm{d}^i}{\mathrm{d}t^i}u^n(x)\Delta t^i + \frac{1}{(k+1)!}\frac{\mathrm{d}^{k+1}}{\mathrm{d}t^{k+1}}u(x,t_*)\Delta t^{k+1}. \tag{4.3}$$

Thus for $k = 1$ we get

$$u^{n+1}(x) = u^n(x) + \frac{\mathrm{d}}{\mathrm{d}t}u^n(x)\Delta t + \frac{1}{2}\frac{\mathrm{d}^2}{\mathrm{d}t^2}u(x,t_*)\Delta t^2.$$

Let $\widetilde{u}$ be the exact solution of the NFL model. Then the truncation error R^n is the residual of the approximation Eq. (4.2) when inserting the exact solution and it is given as

$$R^n(x) = \widetilde{u}^{n+1}(x) - \widetilde{u}^n(x) - \Delta t F[\widetilde{u}^n](x).$$

By inserting the Taylor series of $u^{n+1}(x)$ and using the fact that $\frac{\mathrm{d}}{\mathrm{d}t}\widetilde{u}^n(x) = F[\widetilde{u}^n](x)$ we get

$$\begin{aligned} R^n(x) &= \widetilde{u}^n(x) + \frac{\mathrm{d}}{\mathrm{d}t}\widetilde{u}^n(x)\Delta t + \frac{1}{2}\frac{\mathrm{d}^2}{\mathrm{d}t^2}\widetilde{u}(x,t_*)\Delta t^2 - \widetilde{u}^n(x) - \Delta t\frac{\mathrm{d}}{\mathrm{d}t}\widetilde{u}^n(x) \\ &= \frac{1}{2}\frac{\mathrm{d}^2}{\mathrm{d}t^2}\widetilde{u}(x,t_*)\Delta t^2. \end{aligned}$$

From Lemma 4.2 we get an upper bound of the truncation error

$$\frac{||R^n||_\infty^D}{\Delta t} \leq \frac{1}{2}(C_{tot} + C_\omega)(1 + \beta S'_{\max} C_\omega)\Delta t. \tag{4.4}$$

The truncation error is of *first order* in Δt and the forward Euler method is thus consistent. However, the dependency of β indicates that for large β the necessity for small Δt is apparent.

4.3.2 Convergence

In this section we prove that the forward Euler method applied on the NFL model is convergent. The analysis of convergence is performed in a way analogous to the analysis of a general nonlinear autonomous ODE; see for example Iserles (2009).

Lemma 4.4. *Let t be divided in N_t discrete points t_n with the distance Δt between each point such that $t_{n+1} - t_n = \Delta t = T/N_t$. Further let t_n be defined in the closed interval $Y = [0, T]$ such that $t_0 = 0$ and $t_{N_t} = T$. Let F be continuously differentiable with respect to t on the closed interval $\hat{I} = [t_n, t_{n+1}]\, \forall\, n = 0, 1, 2, ..., N_t$ and differentiable two times with respect to t in the open interval $I = (t_n, t_{n+1})\, \forall\, n = 0, 1, 2, ..., N_t$. Further, assume that $u(t_n, x) = u_n(x)$ is the solution of the NFL model, approximated by the forward Euler approximation given in Eq. (4.2). We denote $\widetilde{u}(t_n, x) = \widetilde{u}^n(x)$ as the exact solution of the NFL model, evaluated at t_n.*

Define the numerical error evaluated at each t_n, $n = 0, 1, 2, ..., N_t$ as $E(t_n, x) = E^n(x) = \widetilde{u}^n(x) - u^n(x)$. Then the numerical error satisfies the following upper bound

$$||E^n||_\infty^D \leq \frac{\Delta t^2 c \beta'}{2} \left(\sum_{k=1}^{n} \binom{n}{k} (\Delta t \beta')^{k-1} \right).$$

Here β' and c are defined as

$$\begin{aligned} \beta' &\equiv 1 + \beta S'_{\max} C_\omega, \\ c &\equiv C_{tot} + C_\omega. \end{aligned} \tag{4.5}$$

Proof. Let

$$E^{n+1}(x) = \widetilde{u}^{n+1}(x) - u^{n+1}(x). \tag{4.6}$$

Then for $u^{n+1}(x)$ we insert the forward Euler approximation (4.2) and expand $\widetilde{u}^{n+1}(x)$ by the use of Taylor's theorem. We denote the exact solution evaluated at t_* as $\widetilde{u}(x, t_*)$ where $t_* \in I$. Then the numerical error is given as

$$\begin{aligned} E^{n+1}(x) &= \widetilde{u}^n(x) + \frac{\mathrm{d}}{\mathrm{d}t}\widetilde{u}^n(x)\Delta t + \frac{1}{2}\frac{\mathrm{d}^2}{\mathrm{d}t^2}\widetilde{u}(x, t_*)\Delta t^2 - u^n(x) - \Delta t F[u^n](x) \\ &= E^n(x) + \Delta t \left(\frac{\mathrm{d}}{\mathrm{d}t}\widetilde{u}^n(x) - F[u^n](x) \right) + \frac{1}{2}\frac{\mathrm{d}^2}{\mathrm{d}t^2}\widetilde{u}(x, t_*)\Delta t^2. \end{aligned}$$

By the substitutions $u^n(x) = \widetilde{u}^n(x) - E^n(x)$ and $\frac{\mathrm{d}}{\mathrm{d}t}\widetilde{u}^n(x) = F[\widetilde{u}^n](x)$ we get

$$E^{n+1}(x) = E^n(x) + \Delta t\big(F[\widetilde{u}^n](x) - F[\widetilde{u}^n - E^n](x)\big) + \frac{1}{2}\frac{\mathrm{d}^2}{\mathrm{d}t^2}\widetilde{u}(x, t_*)\Delta t^2. \tag{4.7}$$

Note that the last part of the r.h.s. of Eq. (4.7) is the truncation error. By the triangle inequality and the lemmas 4.2 and 4.3, the numerical error in t_{n+1} is presented as

$$\begin{aligned} \left|\left|E^{n+1}\right|\right|_\infty^D &\leq ||E^n||_\infty^D + \Delta t(1 + \beta S'_{\max} C_\omega)\, ||E^n||_\infty^D + \frac{1}{2}(C_{tot} + C_\omega)(1 + \beta S'_{\max} C_\omega)\Delta t^2 \\ &= ||E^n||_\infty^D\, (1 + \Delta t(1 + \beta S'_{\max} C_\omega)) + \frac{1}{2}(C_{tot} + C_\omega)(1 + \beta S'_{\max} C_\omega)\Delta t^2. \end{aligned}$$

Then by the definition of β' and c in Eq. (4.5) we get

$$\left|\left|E^{n+1}\right|\right|_\infty^D \leq ||E^n||_\infty^D\, (1 + \Delta t \beta') + \frac{\beta' c}{2}\Delta t^2. \tag{4.8}$$

By using the induction principle we prove that the expression (4.8) implies that

$$||E^n||_\infty^D \leq \frac{\Delta tc}{2}\Big((1+\Delta t\beta')^n - 1\Big). \tag{4.9}$$

The inequality given in Eq. (4.9) can also be expressed by the following binomial representation given as

$$\begin{aligned}
||E^n||_\infty^D &\leq \frac{\Delta tc}{2}\left(\sum_{k=0}^{n}\binom{n}{k}(\Delta t\beta')^k - 1\right)\\
&= \frac{\Delta tc}{2}\left(\binom{n}{0} + \binom{n}{1}(\Delta t\beta')^1 + ... + \binom{n}{n}(\Delta t\beta')^n - 1\right)\\
&= \frac{\Delta t^2 c\beta'}{2}\left(\sum_{k=1}^{n}\binom{n}{k}(\Delta t\beta')^{k-1}\right).
\end{aligned}$$

Let us detail the induction argument leading to (4.9). We let the initial-hypothesis $P(0)$ be given by Eq. (4.8) with $n = 0$. Since the initial condition of Eq. (1.1) is calculated exactly by the forward Euler approximation we get $E^0 = 0$. Thus the initial hypothesis $P(0)$ is

$$\big|\big|E^1\big|\big|_\infty^D \leq \frac{\beta' c}{2}\Delta t^2,$$

which is true for both eqs. (4.8) and (4.9). We further let the induction-hypothesis $P(n)$ be given by Eq. (4.9) and perform the inductive step i.e. $P(n) \to P(n+1)$ by inserting Eq. (4.9) into Eq. (4.8). This gives

$$\begin{aligned}
\big|\big|E^{n+1}\big|\big|_\infty^D &\leq \frac{\Delta tc}{2}\left((1+\Delta t\beta')^n - 1\right)(1+\Delta t\beta') + \frac{\beta' c}{2}\Delta t^2\\
&= \frac{\Delta tc}{2}(1+\Delta t\beta')^{n+1} - \frac{\Delta tc}{2}(1+\Delta t\beta') + \frac{\beta' c}{2}\Delta t^2\\
&= \frac{\Delta tc}{2}\Big((1+\Delta t\beta')^{n+1} - 1\Big).
\end{aligned}$$

□

Theorem 4.1. *Let $||E^n||_\infty^D$ satisfy the bound derived in Lemma 4.4. Then for $N_t = T/\Delta t$ we get*

$$\big|\big|E^{N_t}\big|\big|_\infty^D < \frac{\Delta t}{2}(C_{tot} + C_\omega)\Big(\exp(T)\exp(T\beta S'_{\max}C_\omega) - 1\Big), \quad N_t < \infty. \tag{4.10}$$

Proof. The numerical error $||E^n||_\infty^D$ is smaller than a maximum value of the bound given in Lemma 4.4:

$$\begin{aligned}
||E^n||_\infty^D &\leq \max_{0\leq n\leq N_t}\frac{\Delta tc}{2}\Big((1+\Delta t\beta')^n - 1\Big)\\
&= \frac{\Delta tc}{2}\Big((1+\Delta t\beta')^{N_t} - 1\Big).
\end{aligned}$$

Since $\Delta t = \frac{T}{N_t}$ we get $\Delta t \to 0$ when $N_t \to \infty$. Thus by the limit definition of the exponential function $\mathrm{e}^x = \lim_{n\to\infty}(1+\frac{x}{n})^n$ we get the following chain of inequalities

$$\begin{aligned}
\big|\big|E^{N_t}\big|\big|_\infty^D &\leq \frac{\Delta tc}{2}\Big((1+\frac{T\beta'}{N_t})^{N_t} - 1\Big)\\
&< \frac{\Delta tc}{2}\Big(\exp(T\beta') - 1\Big), \quad N_t < \infty\\
&= \frac{\Delta t}{2}(C_{tot} + C_\omega)\Big(\exp(T)\exp(T\beta S'_{\max}C_\omega) - 1\Big).
\end{aligned} \tag{4.11}$$

The convergence follows trivially in the limit $\Delta t \to 0$. □

If the solution of Eq. (1.1) and its approximation ultimately lie in a bounded set B, then the numerical error estimate given in Eq. (4.10) is pessimistic when $T \to \infty$ and it can be replaced by

$$||E^n||_\infty^D \leq diam(B).$$

Here $diam(B)$ denotes the largest distance between any two points in B (Stuart, 1995).

Corollary 4.1. *If the temporal stepping length Δt satisfies the bound*

$$\Delta t < \frac{2\epsilon}{(C_{tot} + C_\omega)\left(\exp(T)\exp(T\beta S'_{\max} C_\omega) - 1\right)}, \tag{4.12}$$

then the numerical error estimate given in Eq. (4.10) *satisfies* $\left|\left|E^{N_t}\right|\right|_\infty^D < \epsilon$ *with* $\epsilon > 0$.

We see that the upper bound on Δt given in Corollary 4.1 decreases exponentially with the stopping time T, the steepness parameter β and the uniform bound of the connectivity kernel C_ω. Hence, if we insist that Δt satisfies Eq. (4.12) and $0 < \epsilon \ll 1$, then Δt can get very small. This is further illustrated in the following example.

Example 4.1. Let Δt satisfy the bound given in Corollary 4.1. Then for $\epsilon = 0.01$ we get

$$\Delta t < \frac{0.01}{\left(\exp(1)\exp(\frac{300}{2}) - 1\right)} = 2.6 \times 10^{-69},$$

where $T = 1$, $\beta = 300$, $S'_{\max} = \frac{1}{2}$ and $C_{tot} = C_\omega = 1$.

Example 4.1 shows that for global temporal scales, the bound from Theorem 4.1 gives a temporal stepping length Δt which is not practically suitable in approximations as it is much smaller than machine precision. This is because Theorem 4.1 accounts for a worst case scenario where the upper bounds of $\frac{\mathrm{d}^2}{\mathrm{d}t^2}\widetilde{u}(x,t)$ and $|F[u] - F[v]|$ (see lemmas 4.2 and 4.3) are at their respective maximum values for all time t, which they are probably not. However, it is possible that there exists some temporal intervals where this is true, and we discuss and illuminate this further by analysis and numerical experiments in Section 5.

The truncation error plays a prominent role in the numerical error of the forward Euler method. The bound of the truncation error from the forward Euler method has a dependency on β. Further, the third-order temporal derivative given in the proof of Lemma 4.2 has a dependency of β^2 indicating that a second-order RK method will obtain this dependency. Hence, in the next section we derive a second-order RK method and the respective truncation error in order to get a better understanding of the behavior of this method in comparison with the forward Euler method.

4.4 Heun's second order Runge–Kutta method

To approximate Eq. (1.1) by Heun's RK2 method we discretize the temporal variable $t_n = \Delta t n$ and denote $u(x, t_n) = u^n(x), \quad n = 0, 1, 2, ..., N_t$. Furthermore, we denote $t_{n+1} = t_n + \Delta t$ and integrate the NFL model over one time step Δt. The integration yields

$$\int_t^{t+\Delta t} \frac{\partial}{\partial t} u(x,\tau)\,\mathrm{d}\tau = \int_t^{t+\Delta t} F[u](x,\tau)\,\mathrm{d}\tau, \tag{4.13}$$

where F is defined in Eq. (3.3). If we assume that $\frac{\partial}{\partial t}u(x,t)$ is continuous on the closed interval $[t, t+\Delta t]$, then the l.h.s. of Eq. (4.13) can be re-expressed by employing the fundamental theorem of calculus, this gives

$$\int_t^{t+\Delta t} \frac{\partial}{\partial t} u(x,\tau)\,\mathrm{d}\tau = u^{n+1}(x) - u^n(x).$$

The r.h.s of 4.13 is approximated by the trapezoidal rule which is given as

$$\int_{x_0}^{x_N} f(x)\,\mathrm{d}x \approx \frac{\Delta x}{2}(f(x_0) + f(x_n)) + \Delta x \sum_{j=1}^{N-1} f(x_j), \quad \Delta x = \frac{x_N - x_0}{N}.$$

A final result of the approximation in the temporal direction is thus given by the following implicit method given as

$$u^{n+1}(x) = u^n(x) + \frac{\Delta t}{2}(F[u^n](x) + F[u^{n+1}](x)). \tag{4.14}$$

We further discretize the spatial variable x to x_i, $i = 0, 1, 2..., N_x$ such that $u^n(x_i) = u_i^n$, $\Omega = [x_0, x_N]$. We approximate the operator $J[u^n](x)$ given in Eq. (3.2) by the trapezoidal rule over the closed interval $[x_0, x_N]$. We further define the discretized version of F as

$$\mathcal{F}(u_i^n) \equiv -u_i^n + \frac{\Delta x}{2}\big(\omega(x_i, x_0)S(\beta(u_0^n - u_\theta)) + (\omega(x_i, x_N)S(\beta(u_{N_x}^n - u_\theta))\big) + \Delta x \sum_{j=1}^{N_x - 1} \omega(x_i, x_j)S(\beta(u_j^n - u_\theta)).$$

Here $\mathcal{F}(u_i^n) = F[u^n](x)$, $\Delta x \to 0$, and in the succeeding text we only consider the discretized version $\mathcal{F}$. Equation (4.14) is an implicit form known as the Crank–Nicholson method, which we can rewrite in an explicit form by use of the Euler approximation of $\mathcal{F}(u_i^{n+1})$, i.e. we rewrite this part as

$$\mathcal{F}(u_i^{n+1}) = \mathcal{F}(u_i^n + \Delta t \mathcal{F}(u_i^n)).$$

The end result is the the following explicit method given as

$$u_i^{n+1} = u_i^n + \frac{\Delta t}{2}(\mathcal{F}(u_i^n) + \mathcal{F}(u_i^n + \Delta t \mathcal{F}(u_i^n))). \tag{4.15}$$

The method expressed by Eq. (4.15) is known as Heun's method, and it is a predictor-corrector method. The forward Euler method plays the role as the predictor, while the trapezoidal method plays the role as the corrector. This method is also known as a second-order Runge–Kutta method and we rewrite Eq. (4.15) as

$$u_i^{n+1} = u_i^n + \frac{\Delta t}{2}(k_1 + k_2)$$

where

$$k_1 = \mathcal{F}(u_i^n),$$
$$k_2 = \mathcal{F}(u_i^n + \Delta t k_1).$$

This method is divided in two steps, first one 'Euler' step calculating k_1, then one 'trapezoidal' step correcting the 'Euler' step. Thus, if Δt of the forward Euler and the RK2 method is equal, then the RK2 method is less efficient than the forward Euler method. However, the RK2 method is of second order, and in general this allows for a larger Δt than in the forward Euler method, making the RK2 method more efficient.

4.4.1 Consistency

Inserting the exact solution $\widetilde{u}$ of the NFL model into Eq. (4.15) yields the truncation error

$$R^n = \widetilde{u}_i^{n+1} - \widetilde{u}_i^n - \frac{\Delta t}{2}(\mathcal{F}(\widetilde{u}_i^n) + \mathcal{F}(\widetilde{u}_i^n + \Delta t \mathcal{F}(\widetilde{u}_i^n))).$$

Then by Taylors theorem we get

$$\mathcal{F}(\widetilde{u}_i^n + \Delta t \mathcal{F}(\widetilde{u}_i^n)) = \mathcal{F}(\widetilde{u}_i^n) + \Delta t \mathcal{F}(\widetilde{u}_i^n)\frac{\mathrm{d}\mathcal{F}}{\mathrm{d}\widetilde{u}}(\widetilde{u}_i^n) + \frac{\Delta t^2}{2}\mathcal{F}^2(\widetilde{u}_i^n)\frac{\mathrm{d}^2\mathcal{F}}{\mathrm{d}\widetilde{u}^2}(\widetilde{u}_*^*),$$

where $\widetilde{u}_*^* \in (\widetilde{u}_i^n,\ \widetilde{u}_i^n + \Delta t \mathcal{F}(\widetilde{u}_i^n))$. Further, we get

$$\widetilde{u}_i^{n+1} = \widetilde{u}_i^n + \Delta t \frac{\mathrm{d}}{\mathrm{d}t}\widetilde{u}_i^n + \frac{\Delta t^2}{2}\frac{\mathrm{d}^2}{\mathrm{d}t^2}\widetilde{u}_i^n + \frac{\Delta t^3}{6}\frac{\mathrm{d}^3}{\mathrm{d}t^3}\widetilde{u}_i(t_*),$$

where $t_* \in (t_n,\, t_n + \Delta t)$. We also have $\mathcal{F}(\widetilde{u}_i^n) = \frac{\mathrm{d}}{\mathrm{d}t}\widetilde{u}_i^n, \quad \Delta x \to 0$, and in this limit we get the following chain of equalities

$$
\begin{aligned}
&R^n \\
&= \Delta t \frac{\mathrm{d}}{\mathrm{d}t}\widetilde{u}_i^n + \frac{\Delta t^2}{2}\frac{\mathrm{d}^2}{\mathrm{d}t^2}\widetilde{u}_i^n + \frac{\Delta t^3}{6}\frac{\mathrm{d}^3}{\mathrm{d}t^3}\widetilde{u}_i(t_*) - \frac{\Delta t}{2}\left(2\mathcal{F}(\widetilde{u}_i^n) + \Delta t \mathcal{F}(\widetilde{u}_i^n)\frac{\mathrm{d}\mathcal{F}}{\mathrm{d}\widetilde{u}}(\widetilde{u}_i^n) + \frac{\Delta t^2}{2}\mathcal{F}^2(\widetilde{u}_i^n)\frac{\mathrm{d}^2\mathcal{F}}{\mathrm{d}\widetilde{u}^2}(\widetilde{u}_*^*)\right) \\
&= \frac{\Delta t^2}{2}\frac{\mathrm{d}^2}{\mathrm{d}t^2}\widetilde{u}_i^n + \frac{\Delta t^3}{6}\frac{\mathrm{d}^3}{\mathrm{d}t^3}\widetilde{u}_i(t_*) - \frac{\Delta t}{2}\left(\Delta t \frac{\mathrm{d}}{\mathrm{d}t}\widetilde{u}_i^n \frac{\mathrm{d}\mathcal{F}}{\mathrm{d}\widetilde{u}}(\widetilde{u}_i^n) + \frac{\Delta t^2}{2}\left(\frac{\mathrm{d}}{\mathrm{d}t}\widetilde{u}_i^n\right)^2 \frac{\mathrm{d}^2\mathcal{F}}{\mathrm{d}\widetilde{u}^2}(\widetilde{u}_*^*)\right), \quad \Delta x \to 0 \\
&= \frac{\Delta t^3}{6}\frac{\mathrm{d}^3}{\mathrm{d}t^3}\widetilde{u}_i(t_*) - \frac{\Delta t^3}{4}\left(\frac{\mathrm{d}\widetilde{u}}{\mathrm{d}t}(x_i,t_n))\right)^2 \frac{\mathrm{d}^2}{\mathrm{d}\widetilde{u}^2}\frac{\mathrm{d}\widetilde{u}}{\mathrm{d}t}(x_*,t_*)), \quad \Delta x \to 0.
\end{aligned}
$$

Here we denoted $\widetilde{u}(x_i,t_n) = \widetilde{u}_i^n$, $\widetilde{u}(x_*,t_*) = u_*^*$ and used that

$$
\frac{\mathrm{d}\widetilde{u}}{\mathrm{d}t}(x_i,t_n)\frac{\mathrm{d}\mathcal{F}}{\mathrm{d}\widetilde{u}}(\widetilde{u}(x_i,t_n)) = \frac{\mathrm{d}\widetilde{u}}{\mathrm{d}t}(x_i,t_n)\frac{\mathrm{d}}{\mathrm{d}\widetilde{u}}\frac{\mathrm{d}\widetilde{u}}{\mathrm{d}t}(x_i,t_n) = \frac{\mathrm{d}^2}{\mathrm{d}t^2}\widetilde{u}(x_i,t_n), \quad \Delta x \to 0.
$$

We further assume that

$$
\left|\left(\frac{\mathrm{d}\widetilde{u}}{\mathrm{d}t}(x_i,t_n))\right)^2 \frac{\mathrm{d}^2}{\mathrm{d}\widetilde{u}^2}\frac{\mathrm{d}\widetilde{u}}{\mathrm{d}t}(x_*,t_*))\right| \leq \max_{x\in\Omega,\, t\in[0,T]}\left|\frac{\mathrm{d}^3}{\mathrm{d}t^3}\widetilde{u}(x,t)\right|. \tag{4.16}
$$

Then the truncation error satisfies the following inequality

$$
\frac{||R^n||_\infty^D}{\Delta t} \leq \frac{5}{12}\Delta t^2\left(C_\omega + C_{tot}\right)\left(\left(1 + \beta C_\omega S'_{\max}\right)^2 + \beta^2 C_\omega . S''_{\max}\left(C_\omega + C_{tot}\right)\right). \tag{4.17}
$$

We see from Eq. (4.17) that Heun's method is consistent and of *second order*. However, the truncation error contains a second-order exponentiation of the steepness parameter β in the truncation error. This indicates a necessity for small Δt when β is large.

If we demand a maximum value $\epsilon > 0$ of the forward Euler and RK2 bounds given in eqs. (4.4) and (4.17) respectively, we get

$$
\Delta t_E \leq \frac{2\epsilon}{(C_{tot} + C_\omega)(1 + \beta S'_{\max} C_\omega)}, \tag{4.18}
$$

$$
\Delta t_{RK2} \leq \frac{2\sqrt{3/5}\,\epsilon}{\sqrt{\left(C_\omega + C_{tot}\right)\left(\left(1 + \beta C_\omega S'_{\max}\right)^2 + \beta^2 C_\omega S''_{\max}\left(C_\omega + C_{tot}\right)\right)}}. \tag{4.19}
$$

Here the subscripts E, $RK2$ refers to Δt obtained from eqs. (4.4) and (4.17) respectively. In the following example we consider some numerical values of eqs. (4.18) and (4.19).

Example 4.2. Let $\epsilon = 0.001$. Then the temporal stepping lengths obtained in eqs. (4.18) and (4.19) satisfy

$$
\begin{aligned}
\Delta t_E &\leq 6.62 \times 10^{-6}, \\
\Delta t_{RK2} &\leq 3.61 \times 10^{-6},
\end{aligned}
$$

respectively. Here $S'_{\max} = \frac{1}{2}$, $S''_{\max} = \frac{2}{3\sqrt{3}}$, $\beta = 300$ and $C_\omega = C_{tot} = 1$.

By only considering the truncation error, we observe in Example 4.2 that we will not necessarily get a more efficient approximation of the NFL model by using Heun's RK2 v.s. a forward Euler method. This is because the temporal stepping lengths of the two methods are suggested to be almost equally small by the estimates on the bound of the second– and third-order temporal derivative given in Lemma 4.2. However, these estimates accounts for a worst case scenario which is not likely to be close to reality for all values of x, t. In addition, since we do not obtain the numerical error of the RK2 method in this thesis we can only speculate on how efficient it is in reality.

We conjecture that the truncation error has a dependency of β^4 for a RK4 method and β^N for a Nth order RK method. Thus, by the results and assumptions presented in this section it is indicated

that the numerical approximation of the NFL model by the forward Euler and any explicit RK method can require carefully selected temporal stepping lengths. In the next section, we further discuss the numerical analysis of the forward Euler method and indicate that the NFL model can be stiff in parts of its domain of definition. Further, by numerical experiments, we strengthen the hypothesis of stiffness and show that to increase the explicit RK method to fourth order yield no remedy with respect to instability.

5 Results and discussion

In this section we will discuss the results from Section 4 and perform numerical experiments on simplified versions of the NFL model. We begin by introducing an established firing-rate function and discuss different issues in it with regard to numerical error. By this discussion we are directed towards more accurate analysis which again motivates numerical experiments.

5.1 The firing-rate function

We present a firing-rate function obtained from Nielsen et al. (2013) which satisfies the assumptions from Section 3.1 and is given as

$$S(v) = \frac{1}{2}(1 + \tanh(v)). \tag{5.1}$$

The Lipschitz inequality given in Eq. (3.1) of the firing-rate function is a key part in the derivation of the numerical error bound given in Lemma 4.4. The upper bound in the Lipschitz inequality is likely an overestimation for most values of $u, v, \in \mathbb{R}$. Therefore it is interesting to analyze the difference between the l.h.s. and the r.h.s. to get a overview of when these two sides are close. Since the derivative of Eq. (5.1) is at its maximum value $S'_{\max} = \frac{1}{2}$ when the solution of the NFL model is equal to the firing threshold (i.e. $u = u_\theta$; see Fig. 6(A)) we focus the following analysis on this point. Let $v = u \pm \epsilon$ where $\epsilon > 0$. Then the firing-rate function S satisfies the Lipschitz inequality

$$|S(\beta(u - u_\theta)) - S(\beta(u \pm \epsilon - u_\theta))| \leq \beta S'_{\max}\epsilon.$$

Substituting S with Eq. (5.1) yields

$$|\tanh(\beta(u - u_\theta)) - \tanh(\beta(u \pm \epsilon - u_\theta))| \leq \beta\epsilon.$$

Then, if $u = u_\theta$, we get

$$|\tanh(\beta\epsilon)| \leq \beta\epsilon. \tag{5.2}$$

By Fig. 6(B) we observe that in general, $|\tanh(\beta\epsilon)| = o(\beta\epsilon)$ but if $\beta\epsilon \in [0, 0.5 + \delta]$, then $|\tanh(\beta\epsilon)| = \mathcal{O}(\beta\epsilon)$. Here δ is chosen to get a desirable accuracy. Thus, if $\epsilon \leq (0.5 + \delta)/\beta$, then the difference $|S(\beta(u - u_\theta)) - S(\beta(u \pm \epsilon - u_\theta))| - \beta S'_{\max}\epsilon$ is small. This indicates that the real error can be close to the error bound given in Lemma 4.4 when the exact solution of the NFL model is in the proximity of the firing threshold. Notice that $\epsilon \propto 1/\beta$, thus for large β the difference is only small in small intervals ($[u, v]$ or $[v, u]$).

We proceed by analyzing discretization stepping lengths with respect to large steepness parameters β. We define an interval $[u_1, u_2]$ such that $S'(u) \approx 0 \; \forall \; u \notin [u_1, u_2]$; see Fig. 6(A). When β is large, the interval $[u_1, u_2]$ in Fig. 6(A) is small. Hence, in explicit numerical approaches with large β and discretization stepping lengths, the information about change of S inside the interval $[u_1, u_2]$ can be lost. For example, let $[u_0, u_3]$ contain u_1, u_2 with $u_0 < u_1 < u_2 < u_3$. Construct two intervals $I_{1,2} = [u_0, u_3]$ where I_1 consists of four points $\{u_0, u_1, u_2, u_3\}$ corresponding to a large discretization stepping length. Further, let I_2 consist of one thousand scattered points corresponding to a small discretization stepping length. Then the information about change in $S(u)$, $u \in \mathbb{R}$ that lies within $[u_1, u_2]$ is lost for $S(u)$, $u \in I_1$, while much more contained for $S(u)$, $u \in I_2$. Notice that for large β the discretization stepping length must be small to include the points inside $[u_1, u_2]$. Thus for large steepness parameters and discretization stepping lengths, numerical errors are indicated in the proximity of the firing threshold u_θ. Note that outside $[u_1, u_2]$ there is not much change in S and large discretization stepping lengths are indicated to yield less numerical error.

Another reason for inaccuracy in a numerical approach of the NFL model can be round-off error. For large β, the sigmoid S is so steep that a small round-off error of u in the proximity of the firing threshold can yield large errors in computing $S(\beta(u - u_\theta))$. However, the temporal stepping length must be very small in order for round-off errors to be significant. Machine precision is generally around the order of 10^{-15} thus, we do not expect round-off errors to be a significant issue in this study.

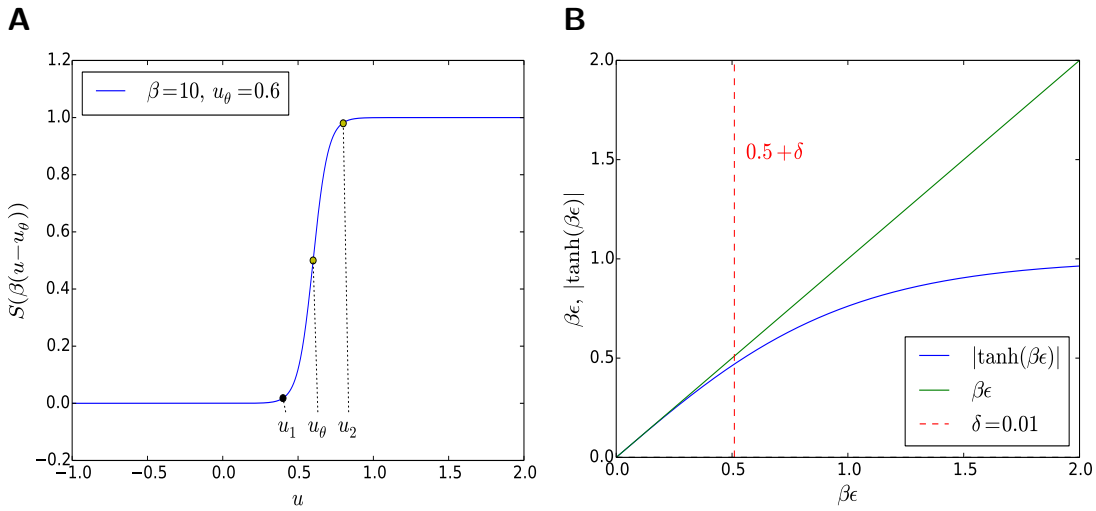

Figure 6: The firing rate function and an evaluation of the Lipschitz inequality at $u = u_\theta$. In (A), the blue line represents the firing-rate function S defined in Eq. (5.1), the dotted lines at u_1 and u_2 represents the neighborhood of the firing threshold u_θ given by the interval $[u_1, u_2]$. In (B) an evaluation of Eq. (5.2) is presented, where the blue and green line represents $\tanh(\beta\epsilon)$ and $\beta\epsilon$ respectively. The region left of the red dashed line represents a neighborhood of u_θ where $|\tanh(\beta\epsilon)| = \mathcal{O}(\beta\epsilon)$, and the region on the right side represents the outside of this neighborhood where $|\tanh(\beta\epsilon)| = o(\beta\epsilon)$.

5.2 Numerical stability of the forward Euler method

In the succeeding text we refer to the firing rate function S given in Eq. (5.1). The discussion in Section 5.1 indicates that numerical errors can occur when the solution of the NFL model is in the proximity of the firing threshold. If $S^{'}(u) \approx S^{'}_{\max}$, then $u \approx u_\theta$. Thus, we can use $S^{'}(u)$ as an *a posteriori* check of when the solution u is in the proximity of the firing threshold u_θ. Hence, we define the following sets

$$\begin{aligned} V_{x,t}(u, u_\theta, \beta, \Gamma) &= \left\{ x \in \Omega,\, t \in [0,T] \,\middle|\, \quad S^{'}(\beta(u(x,t) - u_\theta)) > \Gamma \right\}, \\ W_{x,t} &= u(V_{x,t}(u, u_\theta, \beta, \Gamma)). \end{aligned} \tag{5.3}$$

Definition 5.1. *We define* Γ *such that if* $u(x,t) \notin W_{x,t}$*, then* $\gamma S^{'}(\beta(u(x,t) - u_\theta)) \approx 0 \,\forall\, \gamma < \infty$*. Thus even though* $S^{'}(u) > 0 \,\forall\, u < \infty$*, if* $S^{'}(u) \leq \Gamma$*, then* $S^{'}(u)$ *is zero for all practical purposes, i.e. zero when evaluated by a computer.*

Let $\widetilde{u}$ be the exact solution of the NFL model and let u be an approximation obtained by the forward Euler method. Then the error $E^{n+1}(x) = \widetilde{u}^{n+1}(x) - u^{n+1}(x)$ is given in Eq. (4.7) and consists of three parts given as

$$E^n(x), \tag{5.4}$$

$$\Delta t \left(F[\widetilde{u}^n] - F[\widetilde{u}^n - E^n](x) \right), \tag{5.5}$$

$$\frac{\Delta t^2}{2} \frac{\mathrm{d}^2}{\mathrm{d}t^2} \widetilde{u}(x, t_*),\ t_* \in (t_n, t_n + \Delta t). \tag{5.6}$$

We observe that the error given in Eq. (4.7) can have large values when the three parts in eqs. (5.4) – (5.6) are large and of equal signs. To obtain a better overview of the error $E^{n+1}(x)$ we evaluate Eq. (5.5) by the mean value theorem (see Theorem B.4) and get

$$\begin{aligned} &(F[\widetilde{u}^n] - F[\widetilde{u}^n - E^n])(x) \\ &\quad = E^n(x) + \int_\Omega \omega(x,x')(S(\beta(\widetilde{u}^n(x') - u_\theta)) - S(\beta(\widetilde{u}^n(x') - E^n(x') - u_\theta)))\,\mathrm{d}x' \\ &\quad = E^n(x) + \beta \int_\Omega \omega(x,x') S^{'}(c(x')) E^n(x')\,\mathrm{d}x'. \end{aligned} \tag{5.7}$$

Here $c(x) \in (\widetilde{u}^n, \widetilde{u}^n - E^n)(x)$ or $c(x) \in (\widetilde{u}^n - E^n, \widetilde{u}^n)(x)$. We insert Eq. (5.7) into Eq. (4.7) and get

$$E^{n+1}(x) = E^n(x) + \Delta t\left(E^n(x) + \beta \int_\Omega \omega(x,x') S^{'}(c(x')) E^n(x')\,\mathrm{d}x' \right) + R^n(x). \tag{5.8}$$

Here the truncation error is given as $R^n(x) = \frac{\Delta t^2}{2}\frac{\mathrm{d}^2}{\mathrm{d}t^2}\widetilde{u}(x,t_*)$, $t_* \in (t_n, t_n + \Delta t)$. Since $E^0 = 0$, we see from Eq. (5.8) that the error of the first step is the truncation error, which is given as

$$R^n(x) = \frac{\Delta t^2}{2}\left(-\frac{\partial}{\partial t}\left[\widetilde{u}(x,t_*)\right] + \beta \int_\Omega \omega(x,x') S^{'}(\beta(\widetilde{u}(x',t_*) - u_\theta)) \frac{\partial}{\partial t}\left[\widetilde{u}(x',t_*)\right]\,\mathrm{d}x' \right).$$

Thus if the following points i), ii) and iii) occur simultaneously, then a significantly small Δt seems necessary in order to control the error E^n.

i) $0 \ll S^{'}(c(x')), S^{'}(\beta(\widetilde{u}(x',t_*) - u_\theta)) \leq S^{'}_{\max}$,

ii) β, $\omega(x,x')$ have large values,

iii) $\frac{\partial}{\partial t}\left[\widetilde{u}(x',t_*)\right] \neq 0$.

These points indicate that the NFL model can be stiff if $\widetilde{u}^n(x') \in W_{x,t}$ or if $\widetilde{u}^n(x')$ is close to the boundary of $W_{x,t}$. This is because then $\widetilde{u}(x',t_*)$ can be in the proximity of $0 < u_\theta < 1$ and thus, $c(x')$ can also be in this proximity, depending on the size of the error $E^n(x')$. Note that if $c(x') = 0$, then $S^{'}(c(x')) = S^{'}_{\max}$ and if $\widetilde{u}(x',t_*) = u_\theta$, then $S^{'}(\beta(\widetilde{u}(x',t_*) - u_\theta)) = S^{'}_{\max}$.

If $S^{'}(c(x')), S^{'}(\beta(\widetilde{u}(x',t) - u_\theta)) \leq \Gamma\ \forall\, t > 0, x' \in \Omega$, then the truncation and the numerical error are given as

$$R^n(x) = -\frac{\Delta t^2}{2}\frac{\partial}{\partial t}\left[\widetilde{u}(x,t_*)\right],$$

$$E^{n+1}(x) = E^n(x)(1 + \Delta t) + R^n(x), \tag{5.9}$$

for all practical purposes (see Definition 5.1). However, we must emphasize that this is an idealized proposition and in a real computation this serves as an indication of how the error will behave if $S^{'}(c(x')), S^{'}(\beta(\widetilde{u}(x',t) - u_\theta)) = 0\ \forall\, t > 0, x' \in \Omega$. By a similar induction argument as that presented in the proof of Lemma 4.4 it can be shown that Eq. (5.9) implies

$$E^n = -\frac{\Delta t}{2}\frac{\partial}{\partial t}\left[\widetilde{u}(x,t_*)\right]\left((1 + \Delta t)^n - 1\right). \tag{5.10}$$

Thus, the first-order temporal derivative must be quite large if significant errors are to occur in this regime. The first-order temporal derivative of $\widetilde{u}$ is bounded by $C_{tot} + C_\omega$ (see Lemma 4.1) which value depends on the choice of initial condition and connectivity function. However, it seems unlikely that $\frac{\partial}{\partial t}\left[\widetilde{u}(x,t_*)\right]$ is at its maximum for all $t > 0, x \in \Omega$. Therefore, the NFL model seems non-stiff when $S^{'}(c(x')), S^{'}(\beta(\widetilde{u}(x',t) - u_\theta)) \leq \Gamma$. Further note that the error given in Eq. (5.10) goes to zero if the solution $\widetilde{u}$ reaches a fixed point, thus the asymptotic approximation seems to be good when the solution $\widetilde{u}$ is not in the proximity of the firing threshold u_θ.

The dependency of $\frac{\partial}{\partial t}\left[\widetilde{u}(x',t_n)\right]$ in the truncation error indicates that this error is only significant when the solution $\widetilde{u}$ is changing with time. However, if the truncation error is large when a numerical simulation is initiated, we speculate that this error can consequently shift the approximation u from one basin of attraction to another, making the approximation diverge from the exact solution. Then even if the exact solution reaches a fixed point and the truncation error is zero, the numerical error can be large.

To further evaluate possible numerical errors we assess a situation where the numerical approximation can oscillate. Let $\widetilde{u}(x',t_*) \in W_{x,t}$, $t_* \in (0, \Delta t)$. Then $E^1(x)$ can be large. Assume that $\widetilde{u}(x,t)$ reaches a fixed point in $W_{x,t}$ from $[\Delta t, \infty)$ i.e. $\frac{\partial}{\partial t}\left[\widetilde{u}(x',t_n)\right] = R^n = 0$, $n = 1, 2, 3, \ldots$. If $\widetilde{u}^1(x') - E^1(x') \notin W_{x,t}$, then it is possible that $S^{'}(c(x')) \approx 0$ and the error $E^2(x')$ is reduced. Further, if $\widetilde{u}^2(x') - E^2(x') \in W_{x,t}$, then $E^3(x')$ can be increased, this can make the error and subsequently the

approximating solution oscillate. These predictions are further strengthened by numerical experiments in Section 5.4.

In summary, if $\widetilde{u}^n(x) \notin W_{x,t}$ the numerical approximation will probably converge to the closest attracting limit set. However, it is indicated that large numerical errors can occur when $\widetilde{u}^n(x) \in W_{x,t}$ and the temporal stepping length is not carefully selected. Thus if the error in a previous step e.g. E^1 has shifted $u^1(x)$ away from one basin of attraction to another, then the approximation is indicated to diverge from the exact solution. If the approximation is initiated close to the boundary, or inside $W_{x,t}$, then the numerical error can be large. However, we can not predict the values of $t_*, c(x)$ exactly, therefore in the succeeding text we focus on whether $\widetilde{u}^n(x)$ is inside or outside of $W_{x,t}$. It is further difficult to say much about the limit sets of the NFL model, therefore we will perform a study on a spatially independent version of this model in the next section.

5.3 Numerical experiments on a spatially independent model

The stiffness indicated in Section 5.2 occurs when we address the error in temporal numerical integration. Therefore, it is likely that a spatially independent version of the NFL model will also obtain this stiffness. The spatially independent version of the NFL model is presented as

$$\begin{aligned} \frac{\mathrm{d}}{\mathrm{d}t}u(t) &= f(u(t)), \\ f(u(t)) &= -u(t) + \omega S(\beta(u(t) - u_\theta)), \quad \omega \equiv \omega_0 = const. \\ u(0) &= u_0. \end{aligned} \tag{5.11}$$

The model given in Eq. (5.11) represents a neuronal population which is only subject to input from itself. A positive or negative value of ω determines whether this input is excitatory or inhibitory respectively. We refer the reader to Appendix A for a thorough analysis of the dynamics of Eq. (5.11).

To denote the temporal interval where solutions of Eq. (5.11) is close to the firing threshold u_θ we define the spatially independent set given as

$$V_t(u, u_\theta, \beta, \Gamma) = \left\{ t \in [0, T] \,\middle|\, \beta S^{'}(\beta(u(t) - u_\theta)) > \Gamma \right\}.$$

Here, Γ is defined similarly as in Eq. (5.3); see Definition 5.1. Further, we define the 'global' and 'local' sets

$$\begin{aligned} Q_t &= u([0, T]), \\ W_t &= u(V_t(u, u_\theta, \beta, \Gamma)) \subseteq Q_t. \end{aligned} \tag{5.12}$$

Let $\widetilde{u}$ be the exact solution of Eq. (5.11) and let u be its approximation obtained by the forward Euler method. Then the numerical error is given as

$$E^{n+1} = E^n \left(1 + \Delta t\big(1 + \beta\omega S^{'}(c)\big)\right) + R^n, \tag{5.13}$$

where $c \in (\widetilde{u}^n, \widetilde{u}^n - E^n)$ or $c \in (\widetilde{u}^n - E^n, \widetilde{u}^n)$. The truncation error is defined as

$$R^n = \frac{\Delta t^2}{2} f(\widetilde{u}(t_*))\big(\beta\omega S^{'}(\beta(\widetilde{u}(t_*) - u_\theta)) - 1\big),\ t_* \in (t_n, t_n + \Delta t). \tag{5.14}$$

We observe the appearance of $\beta\omega S^{'}(c)$ and $\beta\omega S^{'}(\beta(\widetilde{u}(t_*) - u_\theta))$ in eqs. (5.13) and (5.14) respectively, indicating a significantly small Δt to be necessary in order to control the error E^n.

5.3.1 Local error

In the succeeding text, we term the numerical error occurring when $\widetilde{u}^n \in W_t$ as the *local error*. Further, when we refer to the forward Euler, the RK2 or the RK4 method, we refer to these methods as they are constructed in the software package ODEsPy (Langtangen and Wang, 2013); see Appendix C for the source code of the experiments.

The analysis in Appendix A demonstrate that Eq. (5.11) can have up to three equilibrium points $u_1 < u_2 < u_3$ where u_1 and u_3 are stable and attractive whereas u_2 is unstable. Further, $u_2 = u_\theta + \mathcal{O}(\delta)$ where δ is small. Thus, if we initiate an approximation of Eq. (5.11) close to u_2, we get $\widetilde{u}^n \in W_t\ \forall\, t \in [0, T_1]$ and $\widetilde{u}^n \notin W_t\ \forall\, t \in (T_1, T_2]$, where $T_{1,2}$ is found experimentally.

We are not able to solve Eq. (5.11) analytically. However, given the result from Corollary 4.1, we can estimate a temporal stepping length Δt_ϵ with a given upper bound of the error denoted ϵ. As a substitute for an exact solution, we approximate Eq. (5.11) with a temporal stepping length Δt_ϵ. Then we measure the numerical error $E^n = \widetilde{u}_\epsilon^n - u^n$ by comparing two approximations: u obtained with $\Delta t = 0.06$ and $\widetilde{u}_\epsilon$ as an 'exact' approximation obtained with Δt_ϵ –both with the forward Euler method. We observe that $\Delta t_\epsilon = 4.4 \times 10^{-18}$ obtained by Corollary 4.1 is practically unusable for $C_\omega = 20$; see Table 5.15. It is observed experimentally (with experiments not shown) that the approximations do not change significantly for $\Delta t_\epsilon < 10^{-5}$ therefore, in the succeeding experiments we set $\Delta t_\epsilon = 6 \times 10^{-5}$.

ϵ	C_ω	C_{tot}	β	T_1	Δt_ϵ
.001	20	20	50	0.06	4.4×10^{-18}
.001	2	2	50	0.06	2.5×10^{-5}

(5.15)

Table 5.15: Explicit values of the temporal stepping length obtained by Corollary 4.1 with parameter values given in the experiments presented in Fig. 7.

The local error is measured in small time intervals ($[0, 0.06]$). Hence, we present the relative error per time unit as

$$E_{rel}^n(\beta) = \frac{E^n}{n\Delta t \widetilde{u}_\epsilon^n}.$$

The relative and numerical errors are observed to be very large (up to $E_{rel}^1 = 2600\%$) even for moderately sized values of β and $|\omega|$; see Table 5.16 and figs. 7(A) and (C). In fact, the numerical approximation is unacceptable for practical purposes when $\widetilde{u}_\epsilon^n \in W_t$ as the approximation is very far from the 'exact' solution. However, it is observed (but not shown) that when $\widetilde{u}_\epsilon \notin W_t$ the approximation tends to the 'exact' solution which is in correspondence to Eq. (5.10). Since the error decreases with time it seems that the asymptotic approximation of Eq. (5.11) is exact for most (small) values of Δt.

T_1	Δt	ω	β	E^1	E_{rel}^1
0.06	0.06	-20	50	0.836	26.18
$0,06$	0.06	2	50	0.024	0.59

(5.16)

Table 5.16: Error obtained from different parameter values of ω, the error and the relative error is measured at the given time T_1. The experiments are graphically illustrated in Fig. 7.

In Section 5.3.3 we further compare the results presented in Table 5.16 to theoretical data obtained in sections 4.3.1 and 4.3.2.

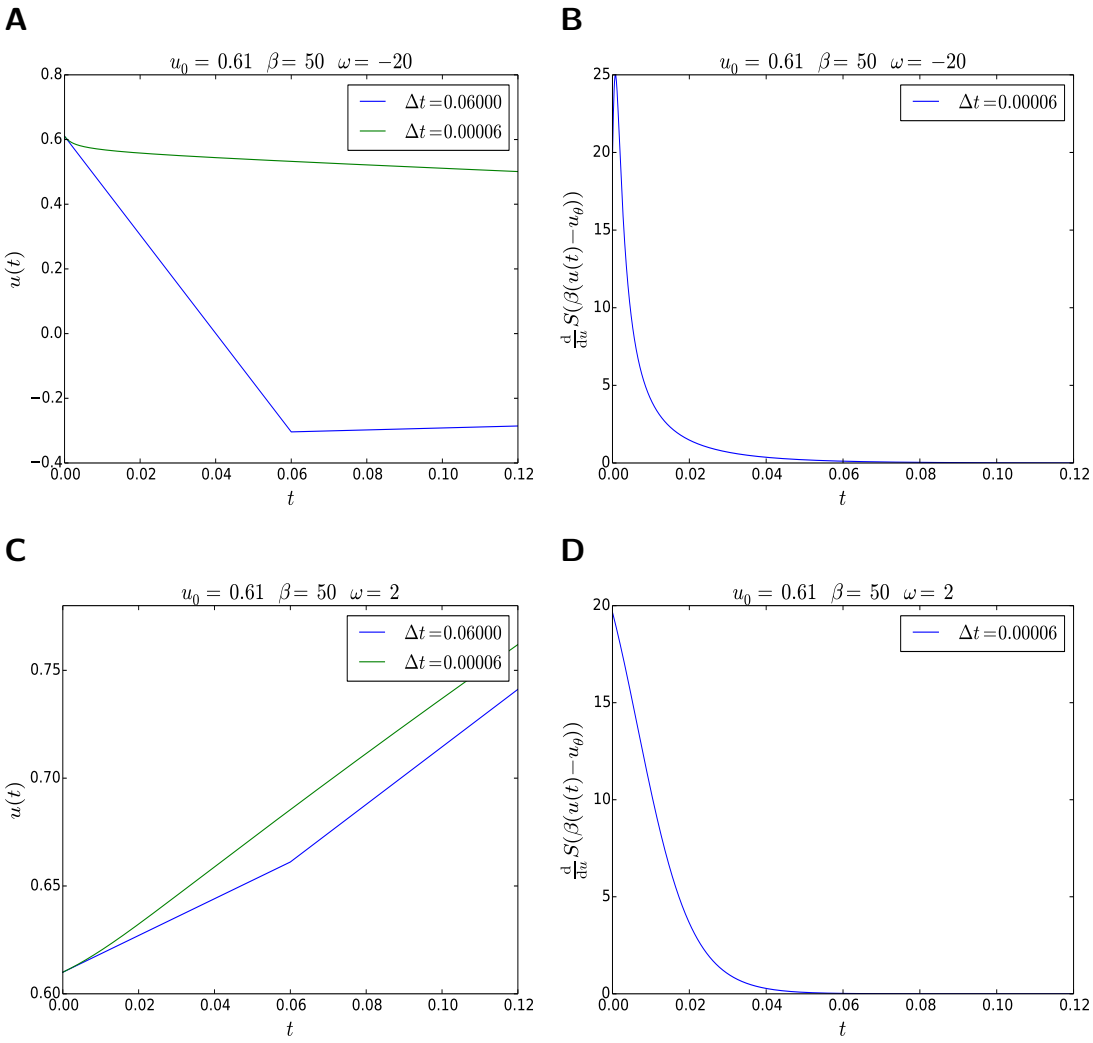

Figure 7: Approximations of Eq. (5.11) for different values of ω. In (A) and (C), the blue and green lines represent the approximative (u) and the 'exact' ($\widetilde{u}_\epsilon$) solutions of Eq. (5.11) respectively. The derivatives of the firing-rate function are presented in (B) and (D), where the nonzero region represents W_t. The stopping times are $T = 0.12$ and the firing thresholds are $u_\theta = 0.6$. Further, the initial conditions u_0, the steepness parameters β and the connectivity constants ω are given in the figure titles.

5.3.2 Convergence estimate in the proximity of the firing threshold

The result from Theorem 4.1 gives an upper bound of the numerical error with an exponential dependency on β. This bound accounts for a worst case scenario in the numerical approximation, and is most likely a large overestimation on a global time scale. However, given the results from sections 5.1 and 5.2 we hypothesize that if $\widetilde{u}$ is in the proximity of u_θ, then there can be stopping times T where the upper bound given in Theorem 4.1 is close to reality. Henceforth, we perform numerical experiments in order to test this hypothesis.

In order to measure the error, we compare two numerical solutions: one from the forward Euler method with a given Δt denoted as u_E and the other from the RK4 method with a much smaller temporal stepping length Δt_ϵ denoted as u_R. The error is measured by taking the difference $E(\beta; T, \Delta t) = |u_R(T) - u_E(T)|$ at the stopping time T for a given Δt and for increasing values of β. Here $\beta \in [\beta_1, \beta_2]$ such that we sample solutions at $\beta + \Delta\beta$. We design the experiments such that the exact solutions of Eq. (5.11) are close to the firing threshold i.e. $\widetilde{u}^{T/\Delta t} \in W_t$.

Figure 8 illustrates that the relative error grows exponentially w.r.t. β. These results indicate that the upper bound of the error given in Theorem 4.1 can be close to reality. Note that the reduction of

$E_{rel}(\beta = 50; \Delta t = 0.06, T = 0.012)$ in Table 5.17 compared to Table 5.16 is due to the reduction in coupling strength ($\omega = 1$).

ω	Δt_ϵ	Δt	$[0, T]$	$E(\beta; \Delta t, T)$	I_β	$\max_{\beta \in I_\beta} E$	$\max_{\beta \in I_\beta} E_{rel}$
1	10^{-5}	0.06	$[0, 0.12]$	$0.0109 \exp(0.024\,\beta) - 0.0290$	$[40, 50]$	0.0072	0.1002
1	10^{-7}	0.01	$[0, 0.01]$	$0.0002 \exp(0.006\,\beta) - 0.0006$	$[200, 300]$	0.00061	0.0805

(5.17)

Table 5.17: Experimental values of the numerical error with respect to different intervals of β and different values of Δt and T. Here $E(\beta; \Delta t, T)$ is presented as a nonlinear curve fit of the measured local error. The maximum values of the numerical error E and the relative error E_{rel} are presented in the last two columns respectively. The temporal stepping lengths Δt_ϵ are used to obtain the 'exact' solutions of Eq. (5.11) and is smallest in the first row corresponding to the smaller value of $\min I_\beta$. The nonlinear curve fits are obtained by the Levenberg–Marquard algorithm through a least squares fitting (Jones et al., 2001).

We proceed by evaluating the *a priori* error bound obtained in Theorem 4.1. If $u_0 < |\omega|$, then $C_{tot} = C_\omega = |\omega|$. Thus by substituting C_{tot} and C_ω by $|\omega|$ in Eq. (4.10), we get a theoretical error bound given as

$$\left|\left|E^{N_t}\right|\right|_\infty^D < \Delta t \left(|\omega| \exp(T) \exp(\frac{T\beta\,|\omega|}{2}) - |\omega| \right). \tag{5.18}$$

We observe that the error obtained experimentally is qualitatively close to the *a priori* estimate given in Theorem 4.1; see tables 5.17 and 5.19. Thus, there are scenarios where Theorem 4.1 can give upper bounds of the error which are relatively close to reality.

ω	Δt	$[0, T]$	$\left\|\left\|E^{N_t}\right\|\right\|_\infty^D(\beta)$	β	$\left\|\left\|E^{N_t}\right\|\right\|_\infty^D$
1	0.06	$[0, 0.12]$	$< 0.0676 \exp(0.060\,\beta) - 0.0600,$	50	< 1.2988
1	0.01	$[0, 0.01]$	$< 0.0101 \exp(0.005\,\beta) - 0.0100,$	300	< 0.0353

(5.19)

Table 5.19: Explicit values of Eq. (5.18) as a function of β (Col. 4) and specific values for given β (Col. 6). Given by two sets of parameter values ω, β, temporal stepping length Δt and stopping time T, that match those of the experiments given in Table 5.17.

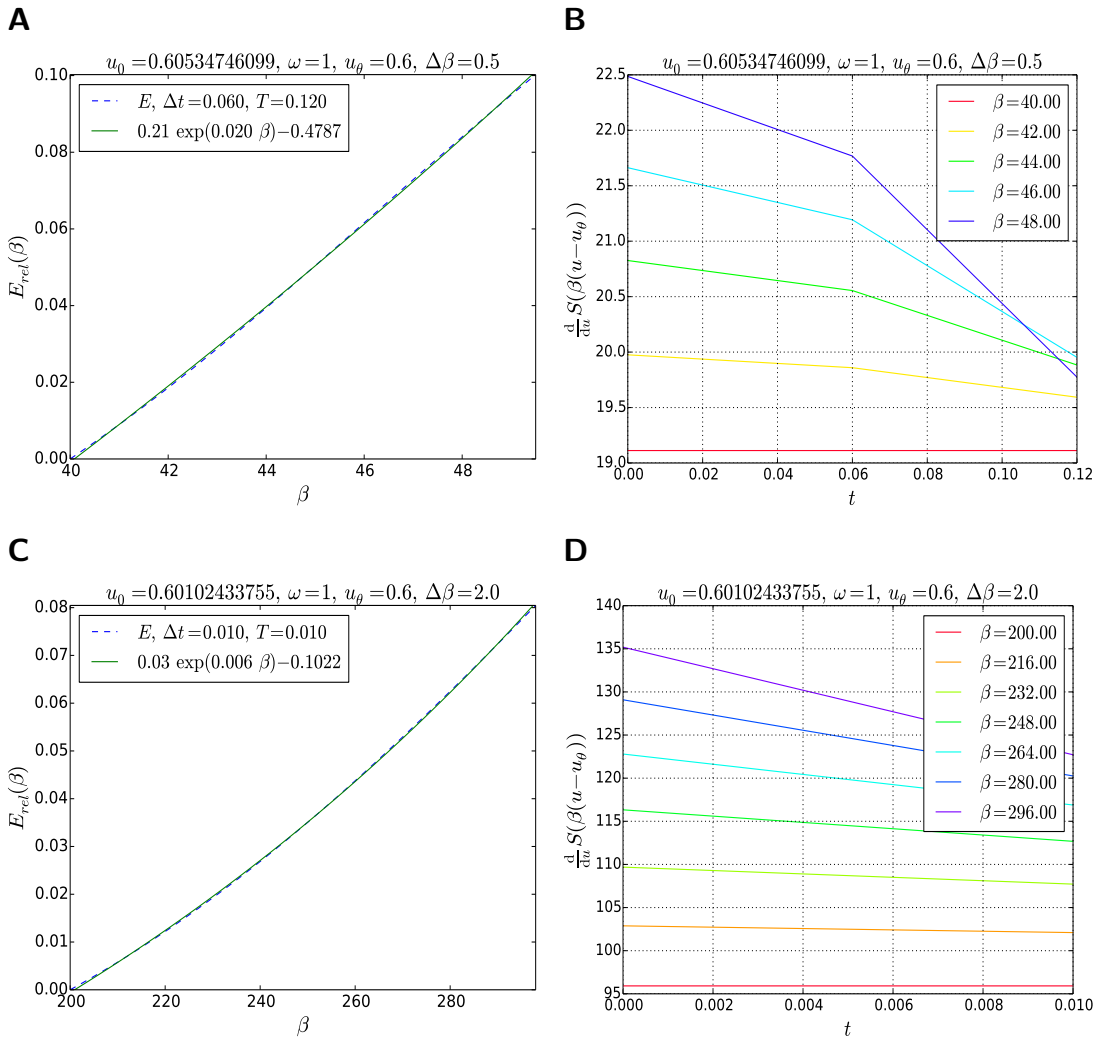

Figure 8: Experimental values of the relative error with respect to different intervals of β. In (A) and (C) the dashed blue and solid green lines represents the relative error and a nonlinear curve fit respectively. The derivatives of the firing-rate function are presented in (B) and (D) where the nonzero region represents W_t. In (A)-(B) the 'exact' RK4 solution and the approximative forward Euler solution are obtained with $\Delta t_\epsilon = 1 \times 10^{-5}$ and $\Delta t = 0.06$ respectively, the steepness parameters are in $\beta \in [40, 50]$. In (C)-(D) the 'exact' RK4 solution and the approximative forward Euler solution are obtained with $\Delta t_\epsilon = 1 \times 10^{-7}$ and $\Delta t = 0.01$ respectively, the steepness parameters are in $\beta \in [200, 300]$. For other simulation parameter values see the figure titles and legends.

5.3.3 Theoretical estimates versus numerical experiments

To assess the difference between the theoretical estimates given in Section 4 and the experimental results given in this subsection we begin by presenting some constants of interest. The solution $\widetilde{u}$ of the NFL model satisfies the uniform bound (see Lemma 3.1) given as

$$|\widetilde{u}(x,t)| \leq C_{tot} = \max(||u_0||_T, C_\omega).$$

The first-order temporal derivative of $\widetilde{u}$ is bounded by $C_\omega + C_{tot}$; see Lemma 4.1. In the case of a spatially independent model with a constant connectivity kernel and a constant initial condition we get

$$||u_0||_T = u_0, \quad C_\omega = |\omega|.$$

If $u_0 < |\omega|$, then $C_{tot} = C_\omega = |\omega|$. However, if $C_\omega \gg u_0$, then C_{tot} can contribute to a large overestimation of $\widetilde{u}^n$ and its first-order temporal derivative in the immediate temporal interval after

$t = 0$. The experimental results given in Table 5.16 illustrates the error after the first temporal step which is equal to the truncation error R_1. We observe in Table 5.20 that the upper bound of the truncation error given in Eq. (4.4) increasingly overestimates the error for larger C_ω.

C_ω	C_{tot}	β	T_1	$\|\|R^n\|\|_\infty^D$	$\|\|R^n\|\|_\infty^D / \widetilde{E}^1$	$\left\|\left\|E^{N_t}\right\|\right\|_\infty^D$
20	20	50	0.06	< 36.072	< 43.162	$< 1.4 \times 10^{13}$
2	2	50	0.06	< 0.367	< 15.223	< 2.439

(5.20)

Table 5.20: Parameter values and corresponding errors from theoretical estimates of the truncation error compared to experimental results (column $5-6$). Finally, in the last column we present a theoretical estimate of the numerical error. The upper bounds of $||R^n||_\infty^D$ and $\left|\left|E^{N_t}\right|\right|_\infty^D$ are obtained from eqs. (4.4) and (4.10) respectively, $\widetilde{E}$ represents the measured error obtained in Table 5.16.

For further evaluation of the estimate given in Theorem 4.1 we assess the exponential approximation of Eq. (4.11) which is good for large values of N_t i.e.

$$\begin{aligned}\left|\left|E^{N_t}\right|\right|_\infty^D &\leq \frac{\Delta t c}{2}\Big((1+\frac{T\beta'}{N_t})^{N_t}-1\Big)\\ &= \frac{\Delta t c}{2}\Big(\exp(T\beta')-1\Big), \quad N_t \to \infty.\end{aligned}$$

When $N_t = 100$ we get $(1+\frac{T\beta'}{100})^{100}$, which is close to $\mathrm{e}^{T\beta'}$ for small values of $T\beta'$, whereas for $N_t = 1$ we get $1 + T\beta'$, and we remind the reader that $\beta' = 1 + \beta S'_{\max} C_\omega$. We thus expect that the result from Theorem 4.1 overestimates the error for small N_t and large $T\beta'$. Hence, explaining the large overestimations of the error presented in the last column of Table 5.20.

5.3.4 Unstable equilibrium points

We have observed that the asymptotic approximations of Eq. (5.11) seems to be exact for most (small) values of Δt. To get a comprehensive overview of the approximations of Eq. (5.11) we proceed by analyzing approximations in an unstable equilibrium point. The model (5.11) can have an unstable equilibrium point u_2 near u_θ (see Appendix A.2). In this point we get a high sensitivity to changes in the temporal stepping length when $u_0 = u_2$. If $f(u_0) = 0$, then $u(t) = u_0 \,\forall\, t$. However, for small perturbations on the initial condition, the solution will tend to one of the stable equilibrium points u_1, u_3. Assume we are able to solve $S(\beta(u_0 - u_\theta)) = u_0$ exact. Then, for the forward Euler method with the first step given as the initial condition i.e. $u^0 = u_0$, we get the following equalities:

$$\begin{aligned}u^1 &= u^0 - \Delta t u^0 + \Delta t S(\beta(u^0 - u_\theta)) = u^0\\ u^2 &= u^0\\ &\vdots\\ u^N &= u^0.\end{aligned}$$

However, due to round-off errors it is possible to get $\Delta t S(\beta(u^0 - u_\theta)) < \Delta t u^0$ in the first Euler step and then the solution will diverge to u_1. On the other hand, if $\Delta t S(\beta(u^0 - u_\theta)) > \Delta t u^0$ in the first Euler step, then the solution diverge to u_3. When $\Delta t S(\beta(u^0 - u_\theta)) = \Delta t u^0$ the solution stays at the initial condition. In Fig. 9 we see a scenario, where two solutions initiated at the same unstable equilibrium point diverge to two different equilibrium points due to a small change in Δt.

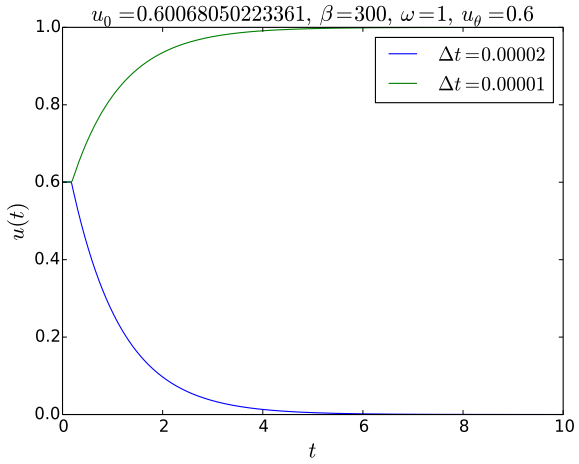

Figure 9: Approximation of Eq. (5.11) on a unstable equilibrium point using two different temporal stepping lengths. The green and blue lines represents approximations initiated with equal parameter values and a small difference in Δt. The simulations are initiated at an approximation of the unstable equilibrium point u_2; see Appendix A.2. For simulation parameters see the figure title.

5.3.5 Global error

We observed in Section 5.3.1 that the local error of the spatially independent NFL model can be of a significant size. We further observed that large global errors can be induced in numerical experiments by choosing the initial condition approximatively equal to the unstable equilibrium point.

To induce large global (asymptotic) errors the local error must shift the approximative solution u from one basin of attraction to another. In the case of a spatially independent model, we can at most have two basins of attraction which are divided by the unstable equilibrium point u_2. If we only change the temporal stepping length Δt, (within reasonable amounts) it is not possible by Lemma 5.1 to shift u from $u^n > u_2$ to $u^n < u_2$. Hence, the asymptotic approximation of Eq. (5.11) is good for all reasonably selected Δt.

Lemma 5.1. *Equation* (5.11) *can have up to three equilibrium points $u_1 < u_2 < u_3$, where u_1, u_3 are stable and u_2 is unstable; see Appendix A. The equilibrium points satisfy:*

$$f(u_i) = 0, \quad i = 1, 2, 3.$$

For large β, the r.h.s of Eq. (5.11) *satisfies the following inequalities:*

$$\begin{aligned} u &\in (u_1, u_2) \quad \Rightarrow \quad f(u) < 0, \\ u &\in (u_2, u_3) \quad \Rightarrow \quad f(u) > 0. \end{aligned}$$

Let the forward Euler sequence be given as

$$u^{n+1} = u^n + \Delta t f(u^n). \tag{5.21}$$

Then if $\Delta t f(u^n) < |u_1 - u^n|$ and $u^0 \in (u_1, u_2)$, we get $u^n < u_2 \, \forall \, n$. Else if $\Delta t f(u^n) < |u^n - u_3|$ and $u^0 \in (u_2, u_3)$, we get $u^n > u_2 \, \forall \, n$.

Proof. The proof will be conducted by the induction principle. Let the initial hypothesis be $u^0 = u(0) \in (u_1, u_2)$, then we get $f(u^0) < 0$ and consequently

$$u^1 = u^0 + \Delta t f(u^0) < u^0 < u_2.$$

Further, assume that $u^n \in (u_1, u_2)$. Then since $f(u^n) < 0$, we get the inductive step:

$$u^{n+1} = u^n + \Delta t f(u^n) < u^n < u_2.$$

For the interval (u_2, u_3) the proof can be conducted in a similar manner. □

In Lemma 5.1 we have a restriction on Δt given by $\Delta t f(u^n) < |u_1 - u^n|$ (and similar for (u_2, u_3)). This is because large Δt can result in large global errors, but these Δt are not of practical interest. Example 5.1 illustrates one possible behavior of large Δt.

Example 5.1. Let $u^0 < u_0$. Then $f(u^0) < 0$. If Δt is so large that in the next step $u^1 < u_1$, then $f(u^1) > 0$. Further, for sufficiently large Δt we get $u^2 > u_3$ which further imply that $f(u^2) < 0$. This pattern will repeat itself and we can get an unbounded numerical approximation u^n oscillating between values less than u_1 and larger than u_3.

However we have only observed the behavior in Example 5.1 for $\Delta t > 1$. In order to obtain a large global error with a reasonable sized Δt we will investigate a more complicated system. We proceed by investigating a neuronal network of two homogeneous populations of neurons.

5.4 Numerical experiments on a coupled pair model

We begin this section with a discretization of the spatial extent Ω in the NFL model by the points x_i, $i = 1, 2, 3, ..., N$. Further, let the operator J defined in Eq. (3.2) be approximated by the rectangular rule. Then the spatially discretized version of the NFL model can be given as

$$\begin{aligned} &\frac{\mathrm{d}u_i}{\mathrm{d}t}(t) = -u_i(t) + \Delta x \sum_{j=1}^{N} \omega_{ij} S(\beta(u_j(t) - u_\theta)), \quad i = 1, 2, 3, ..., N, \\ &u_i(0) = u_{0_i}. \end{aligned} \tag{5.22}$$

Here $\omega(x_i, x_j) = \omega_{ij}$ and gives a constant connectivity between point x_i and x_j. Further, if $N = 2$, then Eq. (5.22) can be reduced to two coupled ODEs given as

$$\begin{aligned} &\frac{\mathrm{d}r}{\mathrm{d}t}(t) = -r(t) + \omega_{rr} S(\beta(r(t) - u_\theta)) + \omega_{rs} S(\beta(s(t) - u_\theta)), \\ &\frac{\mathrm{d}s}{\mathrm{d}t}(t) = -s(t) + \omega_{sr} S(\beta(r(t) - u_\theta)) + \omega_{ss} S(\beta(s(t) - u_\theta)), \\ &r(0) = r_0,\ s(0) = s_0. \end{aligned} \tag{5.23}$$

Here Δx is absorbed into ω_{ij}, $u_1(t) = r(t)$, $u_2(t) = s(t)$, and $r_0 = u_{0_1}$, $s_0 = u_{0_2}$. Equation (5.23) represents a system of two homogeneous populations of neurons; see Fig. 10.

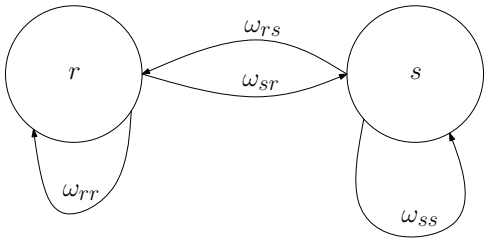

Figure 10: Connectivity between two coupled homogeneous neuron populations r and s. Here ω_{rs} denotes the coupling strength from s to r.

The system given in Eq. (5.23) is constructed according to Dale's principle[4] where s is an excitatory and r is an inhibitory population. The population s is primarily self-excited and coupled as strongly excitatory to the population r with a minor inhibitory feedback to s in addition, r is strongly self-inhibitory. We denote $\widetilde{r}$, $\widetilde{s}$ as the exact and r, s as the approximated solutions of Eq. (5.23). As we do not obtain the exact solutions $\widetilde{r}$, $\widetilde{s}$ these are approximated by the RK4 method using a small Δt_ϵ which is found experimentally. These solutions are henceforth referred to as 'exact' solutions and denoted as $\widetilde{r}_\epsilon$, $\widetilde{s}_\epsilon$. The experiments are conducted with a moderately sized steepness parameter and with different sizes of the temporal stepping lengths Δt, graphically illustrated in figs. 11 – 13. The experiments demonstrate a significant numerical error when solving Eq. (5.23) by the RK4 method when $\widetilde{r}_\epsilon(t) \in W_t$.

We find a set of parameter values that induce a scenario presented in figs. 11(A) and (B) where the initial error shifts the approximation from one basin of attraction to another, such that it diverges from the 'exact' solution. By reducing Δt, we further observe in Fig. 11(D) a spurious fixed point produced by the RK4 method. This type of behavior in RK methods has previously been observed by Iserles (1990). It should be noted that the spurious fixed point occurs when the temporal stepping length is small compared to commonly used values in the literature (see e.g. Faye and Faugeras (2010); Nielsen et al. (2013)). In addition, the approximation has a smooth and coherent appearance indicating that these types of numerical errors can be difficult to identify in approximations.

In Fig. 12 we change the initial value of s and observe that a false oscillation occurs. The oscillation is also observed in an approximation by the forward Euler method, strengthening the prediction done in Section 5.2 regarding oscillatory numerical errors. The selected temporal stepping length causes the approximation to oscillate with a frequency closely related to the stepping length. It is observed

[4]Dale's principle indicates that $\mathrm{sign}(\omega_{rr}) = \mathrm{sign}(\omega_{sr})$ and $\mathrm{sign}(\omega_{ss}) = \mathrm{sign}(\omega_{rs})$.

that for the forward Euler method with $\Delta t = 0.01$ and no feedback from r to s, the frequency of the oscillations is $f = \frac{1}{2\Delta t}$. For the RK4 method the relation between the frequency and Δt is more complex but appears to be closely related, as seen in Fig. 13(B). It is further observed in Fig. 13 that by reducing the feedback from r to s ($\omega_{sr} = 0$), the instability is isolated to r where $\widetilde{r}_\epsilon^n \in W_t$. This is corresponding with the hypothesis in Section 5.2 that the NFL model is stiff when $\widetilde{u}(x', t) \in W_{x,t}$.

In order to analyze the stability of the fixed points presented in figs. 11 – 13 we present the Jacobian of Eq. (5.23) as

$$J(r(t), s(t)) = \begin{bmatrix} \frac{\beta\omega_{rr}}{2}\left(-\tanh^2\left(\beta\left(r(t) - u_\theta\right)\right) + 1\right) - 1 & \frac{\beta\omega_{rs}}{2}\left(-\tanh^2\left(\beta\left(s(t) - u_\theta\right)\right) + 1\right) \\ \frac{\beta\omega_{sr}}{2}\left(-\tanh^2\left(\beta\left(r(t) - u_\theta\right)\right) + 1\right) & \frac{\beta\omega_{ss}}{2}\left(-\tanh^2\left(\beta\left(s(t) - u_\theta\right)\right) + 1\right) - 1 \end{bmatrix} \tag{5.24}$$

The Jacobian at $T = 60$ with the parameters used in in figs. 11 – 13, are given as

$$J(\widetilde{r}_\epsilon(T), \widetilde{s}_\epsilon(T)) = \begin{bmatrix} -686.64 & 0.0 \\ -137.13 & -1.0 \end{bmatrix}, \quad \begin{bmatrix} -686.64 & 0.0 \\ -137.13 & -1.0 \end{bmatrix}, \quad \begin{bmatrix} -686.64 & 0.0 \\ 0.0 & -1.0 \end{bmatrix}$$

respectively. The fixed points of the 'exact' solutions $\widetilde{r}_\epsilon$, $\widetilde{s}_\epsilon$ presented in in figs. 11 – 13 thus represents stable hyperbolic fixed points as they yield negative real eigenvalues of the Jacobian (5.24).

To assess stiffness we present the stiffness index, defined as

$$L = \max |Re(\lambda_i)|$$

(Shampine and Thompson, 2007). Here $Re(\lambda_i)$ denotes the real part of a Jacobian eigenvalue. The stiffness index is $L = 686.64$, indicating that the parameter values used in figs. 11 – 13 is part of a stiff parameter space of Eq. (5.23).

When Δt is selected within reasonable sizes i.e. $\Delta t \ll 1$ there are no indications of unbounded errors occurring. However, we observe large numerical errors in Eq. (5.23) causing the computational results to be practically unusable. We further raise the question of whether similar instabilities can occur in explicit approximations of the full NFL model, i.e. for a non-constant connectivity function and $N \gg 2$ in Eq. (5.23). We observe that the discussion in Section 5.2 highlights many of the presented numerical errors obtained in the experiments performed in sections 5.3 and 5.4. Thus, we speculate that this discussion also highlights similar numerical errors in the full NFL model.

The temporal stepping length of 0.06 and the steepness parameter $\beta = 50$ used in most of the experiments presented in this thesis are obtained values from Faye and Faugeras (2010). Here a temporal delay version of the NFL model was studied with a temporal stepping length $\Delta t = h = 0.0667$ and steepness parameters $\beta \leq 45$. The models presented in this thesis are different than the temporal delay version, thus the instabilities presented in this thesis are not necessarily obtained in Faye and Faugeras (2010). However, the results obtained in this thesis suffices to call for a stability analysis on any numerical approach employed on the NFL (and similar) model(s).

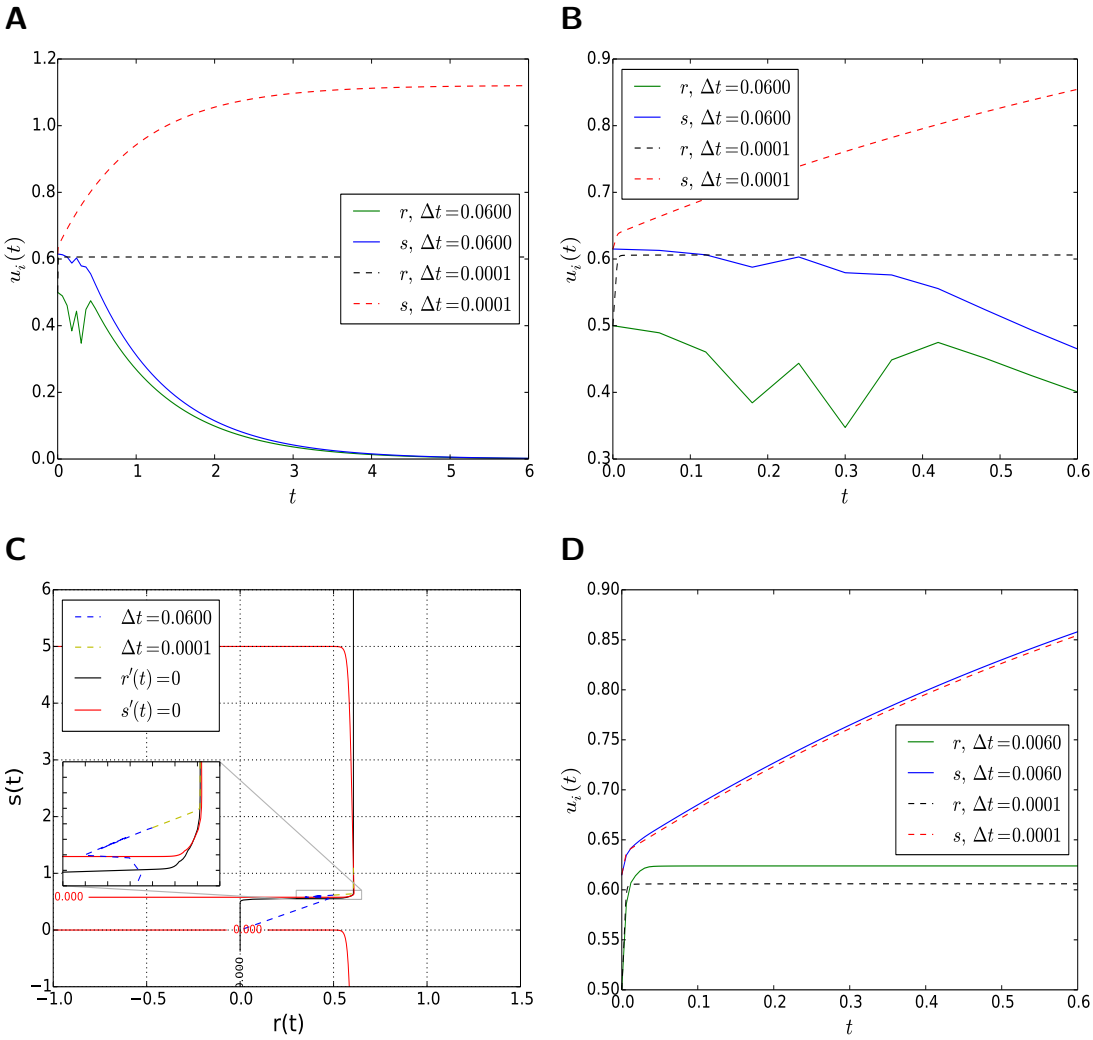

Figure 11: Results from the two population model given in Eq. (5.23) approximated by the RK4 method. A time evolution is presented in (A) with a close up given in (B). Here the solid and the dashed lines represent the approximative and the 'exact' solutions respectively. A phase plane is presented in (C) where solid lines express nullclines, and intersections of nullclines represent fixed points of Eq. (5.23). Further, dashed lines represent trajectories where the yellow and blue lines are representing the approximative and the 'exact' solutions respectively. For $\Delta t = 0.006$ a spurious solution occurs, illustrated by the green line in (D). The initial conditions are $s_0 = 0.615$, $r_0 = 0.5$, the firing threshold is $u_\theta = 0.6$, the synaptic weights are $\omega_{rr} = -30, \omega_{rs} = 20, \omega_{ss} = 5, \omega_{sr} = -6$ and the steepness parameter is $\beta = 50$.

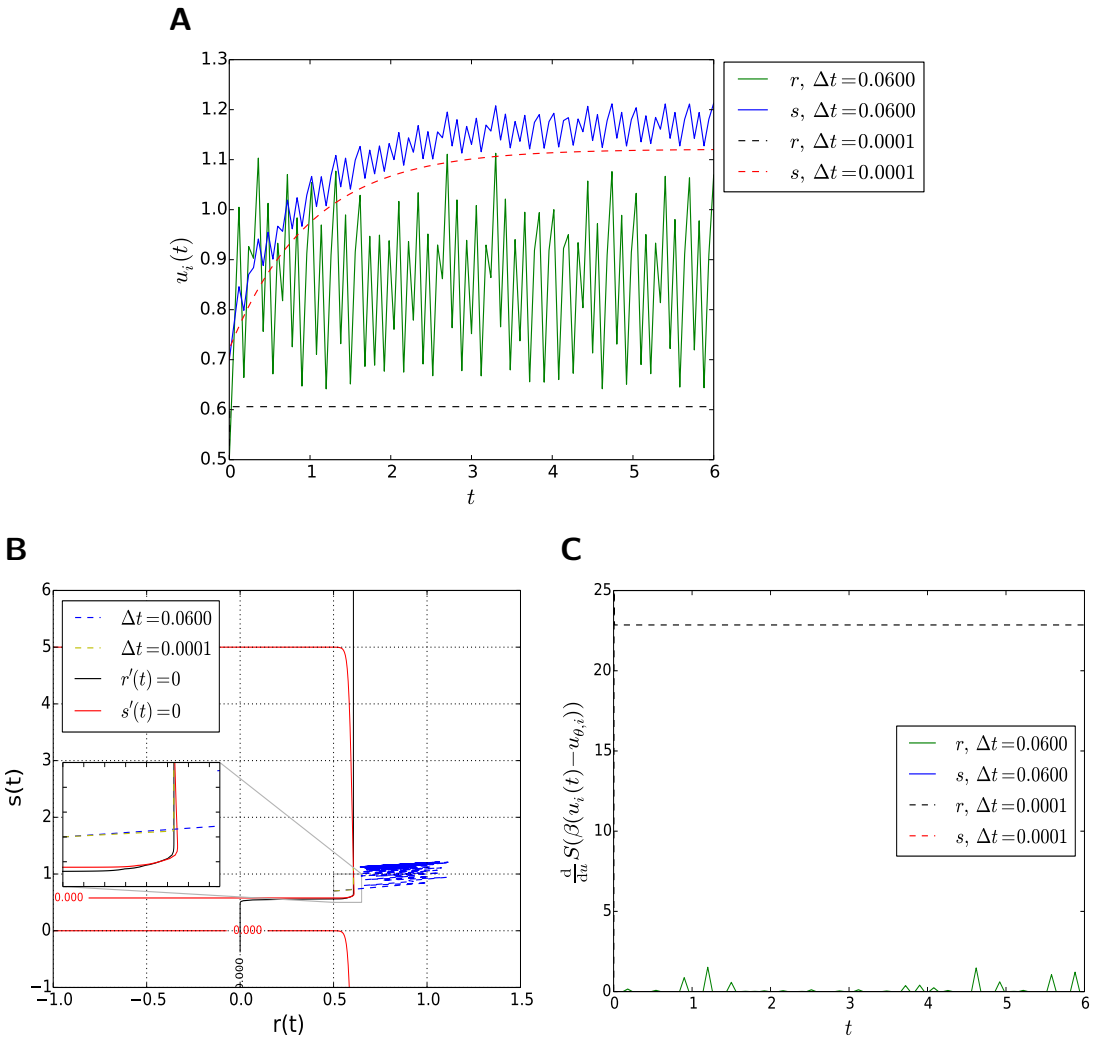

Figure 12: Results from the two population model given in Eq. (5.23) approximated by the RK4 method where the initial conditions are changed (w.r.t. Fig. 11) to $s_0 = 0.7$, $r_0 = 0.5$. A time evolution is presented in (A) where the solid and the dashed lines represent the approximative and the 'exact' solutions respectively. A phase plane is presented in (B) where solid lines express nullclines, and intersections of nullclines represent fixed points of Eq. (5.23). Further, dashed lines represent trajectories where the yellow and blue lines are representing the approximative and the 'exact' solutions respectively. The derivatives of the firing-rate function are presented in (C) where the nonzero region represent $\in W_t$ for values over 0. The firing threshold is $u_\theta = 0.6$, the synaptic weights are $\omega_{rr} = -30, \omega_{rs} = 20, \omega_{ss} = 5, \omega_{sr} = -6$ and the steepness parameter is $\beta = 50$.

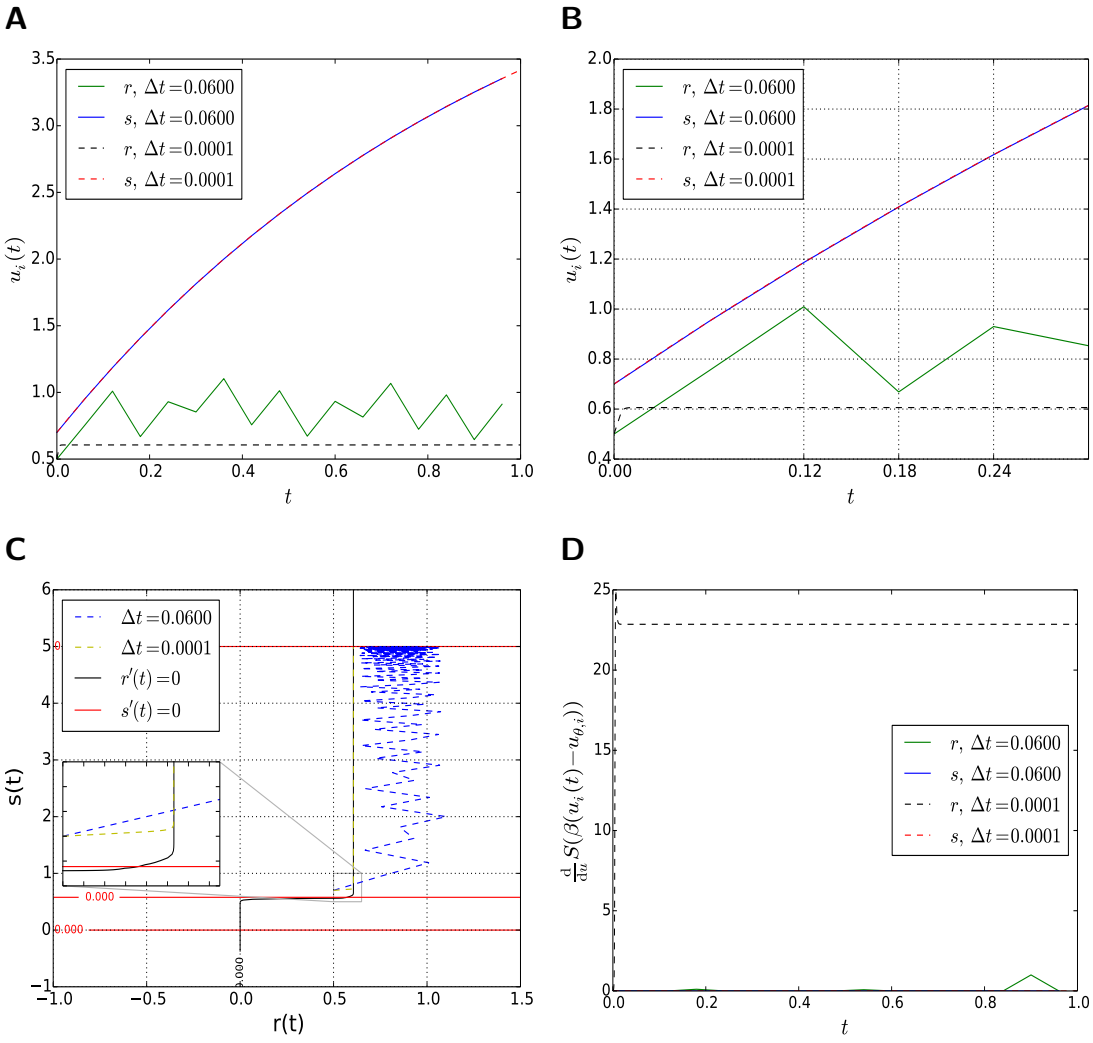

Figure 13: Results from the two population model given in Eq. (5.23) approximated by the RK4 method where where the synaptic weights are changed (w.r.t. Fig. 12) to $\omega_{rr} = -30, \omega_{rs} = 20, \omega_{ss} = 5, \omega_{sr} = 0$; shutting off the inhibitory feedback from r to s. A time evolution is presented in (A) with a close up given in (B). Here the solid and the dashed lines represent the approximative and the 'exact' solutions respectively. A phase plane is presented in (C) where solid lines express nullclines, and intersections of nullclines represent fixed points of Eq. (5.23). Further, dashed lines represent trajectories where the yellow and blue lines represent the approximative and the 'exact' solutions respectively. The derivatives of the firing-rate function are presented in (D) where the nonzero region represent $\in W_t$. The initial conditions are $s_0 = 0.7$, $r_0 = 0.5$, the firing threshold is $u_\theta = 0.6$ and the steepness parameter is $\beta = 50$.

6 Concluding remarks and outlook

6.1 Concluding remarks

We reviewed the derivation and a well-posedness proof of the NFL model equipped with a sigmoidal firing-rate function: the model is well posed in the sense of Hadamard, with a poor stability estimate. The biophysical derivation indicates that the NFL model is an extrapolation of the integrate and fire network; from a finite to an infinite dimensional system. It seems that the most suitable approach of analysis is obtained from theory for ODEs. Theory for ODEs appears to provide a simple and well established set of tools with respect to analysis of numerical properties and well-posedness. The current argumentation on re-casting the NFL model as a higher order nonlinear PDE seems insufficient with respect to theory of well-posedness and numerical analysis. However, the PDE formalism may well prove merits that are out of the scope of this thesis.

When assessing the numerical properties of the NFL model it was observed that the forward Euler method is consistent and convergent. An upper bound of the numerical error was observed exponentially dependent on β, C_ω and T. The upper bound of the numerical error suggested Δt to be impractically small on a global time scale. This indicates that the error bound is not practically suitable to predict what size of the temporal stepping length to use in approximations. We further observed consistency of Heun's RK2 method. However, the truncation error was observed to contain β^2, indicating a weakened efficiency of this method when compared to the forward Euler method.

Performed analysis indicated that the NFL model is stiff when its solution is in the proximity of the firing threshold. Further, no remedy w.r.t. stiffness were indicated when the order of the explicit RK methods was increased. The NFL model seemed non-stiff when its solution was appropriately far away from the firing threshold.

These indications were further strengthened by numerical experiments where the temporal stepping lengths were selected according to relevant literature. Significant errors were observed in approximations by the forward Euler method on a spatially independent version of the NFL model. Furthermore, numerical analysis on a coupled pair version of the NFL model was performed by the RK4 method. The approximations revealed a worst case scenario where the approximation were shifted from one basin of attraction to another, resulting in a divergence from the exact solution. Further, we found a parameter set that yielded false oscillations in the approximation, and when reducing Δt a false fixed point occurred. Based on these results we indicate difficulties in recognizing errors occurring when approximating the NFL model in the proximity of the firing threshold. Results further indicated that the asymptotic approximations were correct when the solution was not in the proximity of the firing threshold. Finally, for the selected temporal stepping lengths, round-off errors seem to be insignificant both locally and asymptotically, except for approximations of unstable limit sets.

6.2 Outlook

There are evidence given in this thesis not to trust computational output of NFL type models where the temporal stepping lengths are not carefully selected. We underline that the stiffness probably span a large range of firing-rate models where the firing-rate function is similar to the one used in this thesis.

It can be a complicated endeavor to predict all situations where the solution of the NFL model is in the proximity of the firing threshold. The easiest numerical approach is probably an adaptive numerical scheme which can reduce the discretization stepping length when the solution is in the proximity of the firing threshold. However, we observed a possibility for the solution of the NFL model to stay close to the firing threshold value for all time. Thus in this regime, efficient schemes can be hard to derive. Implicit schemes such as the backward Euler or the trapezoidal methods are known to be A-stable and can be solved by e.g. Newtons method. However, these methods can be computationally costly since it is necessary to solve large sets of nonlinear equations. These and other multi-step methods deserve to get a thorough analysis with regard to solving the NFL model. However, these methods are not likely to provide sufficiently efficient approximations. It may well be that one gets more stable numerical methods by a PDE formalism of the NFL model, but given the numerical instability encountered in this thesis there seems to be a need for justifications of the numerical stability for any type of model similar to the NFL model.

The NFL model has a reduced biophysical complexity, and is well suited to give an easy computational implementation. The complications observed in this thesis regarding numerical approximations

seems to undermine this simplicity. Thus, for future analysts we suggest focus on developing other types of neural field models which are more robust with respect to numerical approximations.

Acknowledgement

A special thank is in order for Maria Hultman and Eivind Hennestad which help regarding the writing of this thesis was very appreciated. In addition, a thank goes to the contributors of the excellent open software packages Ipython, SciPy, Matplotlib, SymPy, and ODEsPy; see Pérez and Granger (2007); Jones et al. (2001); Hunter (2007); SymPy Development Team (2014); Langtangen and Wang (2013). Let the Internet and all science software be free and open! 'Freedom, the first-born of science.' –Thomas Jefferson

Appendix A Pseudo exact solution

A.1 Derivation

In this appendix we will find a regularly perturbed system, approximating Eq. (5.11) for large steepness parameters. To this end we substitute $v = S(\beta(u-u_\theta))$ with the firing-rate function given in Eq. (5.1) i.e.

$$v(t) = \frac{1}{2}(1 + \tanh(\beta(u(t) - u_\theta))).$$

Here $0 < v < 1$ and a solution for u is thus

$$u = u_\theta + \varepsilon\frac{1}{2}\log(\frac{v}{1-v}), \quad \varepsilon = \frac{1}{\beta}. \tag{A.1}$$

The new parameter ε is referred to as the *inverse steepness parameter* and we notice that the limit $\beta \to \infty$ corresponds to $\varepsilon \to 0$. By inserting Eq. (A.1) into Eq. (5.11) we obtain the following dynamical system

$$\begin{aligned} \varepsilon\frac{\mathrm{d}}{\mathrm{d}t}v(t) &= -2\omega(v - v_\theta)(v-1)v - \varepsilon\psi(v), \quad v_\theta = \frac{u_\theta}{\omega} \\ v(0) &= v_0. \end{aligned}$$

Here the initial condition is $v_0 = \frac{1}{2}(1 + \tanh(\beta(u_0 - u_\theta)))$ and the function ψ is defined as

$$\begin{aligned} \psi(v) \equiv v(1-v)\log(\frac{v}{1-v}) &= v(1-v)\log(v) - v(1-v)\log(1-v) \\ &= (1-v)f(v) - vf(1-v), \quad f(x) = x\log(x). \end{aligned} \tag{A.2}$$

We further introduce the time stretching transformations

$$\tau = \frac{t}{\delta}, \quad \delta = \frac{\varepsilon}{2\omega}, \quad V(\tau) = v(t) \tag{A.3}$$

and end up with the system

$$\begin{aligned} \frac{\mathrm{d}}{\mathrm{d}\tau}V &= -(V - v_\theta)(V-1)V - \delta\psi(V) \\ V(0) &= v_0. \end{aligned} \tag{A.4}$$

By substituting the time stretching transformations defined in Eq. (A.3) into (5.11) we get

$$\begin{aligned} \frac{\mathrm{d}}{\mathrm{d}t}u(\tau) &= -\delta u(\tau) + \delta\omega\frac{1}{2}(1 + \tanh(\beta(u(\tau) - u_\theta))) \\ u(0) &= u_0. \end{aligned} \tag{A.5}$$

The dynamical system (A.4) is a regular perturbed system where δ plays the role as the perturbation parameter. More importantly, since

$$\lim_{V\to 0^+}\psi(V) = 0, \quad \lim_{V\to 1^-}\psi(V) = 0,$$

ψ can be extended to a continuous and bounded function on the closed interval $[0, 1]$. Thus $\delta\psi$ will be of order ε for $0 \leq V \leq 1$ and uniformly small for $0 < \delta \ll 1$. The evaluation of ψ is illustrated graphically in Fig. 14 indicating that we may omit the term $\delta\psi(V)$ for large β. The resulting equation is presented as

$$\begin{aligned} \frac{\mathrm{d}}{\mathrm{d}\tau}V(\tau) &= f(V(\tau)) \\ f(V(\tau)) &= -(V(\tau) - v_\theta)(V(\tau)-1)V(\tau) \\ V(0) &= v_0 \end{aligned} \tag{A.6}$$

Equation (A.6) has three equilibrium points i.e. where $f(V) = 0$, here the dynamics can be different between eqs. (A.4) and (A.6) since $f(V) \approx \delta\psi(V)$. By further evaluation presented in Appendix A.2 we observe that Eq. (A.4) has two stable equilibrium points and one unstable equilibrium point which

are all hyperbolic. Thus for large β, Eq. (A.6) is a leading order approximation of Eq. (A.4). The exact solution of Eq. (A.6) is given as

$$\tau = \frac{1}{v_\theta\,(v_\theta - 1)} \left(v_\theta \log\left(\frac{v_0\,(V(\tau) - 1)}{V(\tau)\,(v_0 - 1)} \right) + \log\left(\frac{V(\tau)\,(v_0 - v_\theta)}{v_0\,(V(\tau) - v_\theta)} \right) \right). \tag{A.7}$$

Equation (A.7) is an implicit equation we can solve by Newtons method, giving an almost exact solution of Eq. (A.6). Due to structural stability this solution qualitatively approximates the solution of (A.5). However, this approximation is not necessarily accurate in size because of the error done by neglecting the term $\delta\psi(V)$ in Eq. (A.4). To assess this simplification-error we compare the numerical solution of Eq. (A.4) and Eq. (A.6) which is of order 1×10^{-1}. Thus, Eq. (A.7) does not provide any better approximation of the exact value of Eq. (5.11) than what is obtained by a numerical approximation of Eq. (5.11) with a small temporal stepping length.

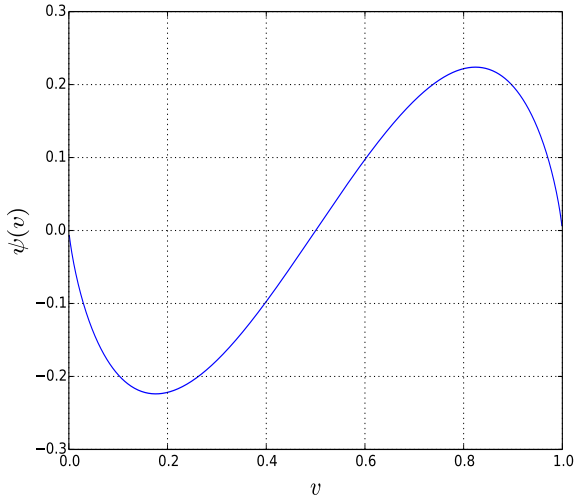

Figure 14: The function ψ is represented by the blue line with maximum values at ca. $[-0.224, 0.224]$.

A.2 Stability of the spatial independent NFL model

In this appendix we want to extract as much information as possible from the regular perturbed version of Eq. (5.11), given as

$$\begin{aligned} V_\tau &= F(V, \delta) \\ F(V, \delta) &= f(V) - \delta\psi(V), \quad 0 < \delta \ll 1 \\ f(V) &= -(V - v_\theta)(V - 1)V. \end{aligned} \tag{A.8}$$

The term $\delta\psi(V)$ in Eq. (A.8) is defined in Eq. (A.2) and can be neglected when $|\delta\psi(V)| \ll |f(V)|$. This can be done for all $V \in [0, 1]$ except for the interval where $V = v_\theta + \mathcal{O}(\delta)$. The endpoints are analyzed by inserting a perturbation about these equilibrium points by the perturbation given as

$$V = V_{eq} \pm \delta\widetilde{V}, \quad 0 < \delta \ll 1, \quad V_{eq} \in \{0, 1\}.$$

By inserting the perturbation we get

$$\delta\widetilde{V}_\tau = -(V_{eq} \pm \delta\widetilde{V} - v_\theta)(V_{eq} \pm \delta\widetilde{V} - 1)(V_{eq} \pm \delta\widetilde{V}) - \delta\psi(V_{eq} \pm \delta\widetilde{V}). \tag{A.9}$$

We can thus observe that Eq. (A.9) yields

$$\begin{aligned} &\text{for } V = \delta\widetilde{V}, && \text{for } V = 1 - \delta\widetilde{V}, \\ &f(V) = \mathcal{O}(\delta), && f(V) = \mathcal{O}(\delta), \\ &\psi(V) = \psi(\delta V) \to 0, \delta \to 0, && \psi(V) = \psi(1 - \delta V) \to 0, \delta \to 0. \end{aligned}$$

Thus, the points $V_{eq} = 0$, 1 are stable equilibrium points. Further we observe that

$$\begin{aligned} F &\in C^2((0, 1) \times \mathbb{R}) \\ F(V, 0) = 0 &\iff V = v_\theta \\ &\left[\frac{\partial F}{\partial V} \right] (v_\theta, 0) \neq 0. \end{aligned}$$

The implicit function theorem guarantees a unique solution $V = g(\delta)$ of the equation $F(V, \delta) = 0$ in the interval $I_\delta = [-\delta_1, \delta_2]$ where $0 \in I_\delta$. We further linearize $g(\delta)$ around $\delta = 0$, and get

$$V = v_\theta + \delta v_1 + ..., \quad \delta \in I_\delta.$$

By further Taylor expanding $F(V, \delta)$ around $(v_\theta, 0)$ we get

$$F(V, \delta) = F(v_\theta, 0) + \frac{\partial F}{\partial V}(v_\theta, 0)\delta v_1 + \frac{\partial F}{\partial \delta}(v_\theta, 0)\delta + ... = 0.$$

Here we used the fact that $F(v_\theta + \delta v_1 + ..., \delta) = 0$, thus

$$\frac{\partial F}{\partial V}(v_\theta, 0)v_1 + \frac{\partial F}{\partial \delta}(v_\theta, 0) = 0.$$

Hence the expression for v_1 is

$$v_1 = -\frac{\frac{\partial F}{\partial \delta}}{\frac{\partial F}{\partial V}}(v_\theta, 0) = -\frac{\psi(v_\theta)}{v_\theta(1 - v_\theta)} = \log\left(\frac{1 - v_\theta}{v_\theta}\right).$$

The linearized expression for $g(\delta)$ is

$$g(\delta) \approx v_\theta + \delta \log\left(\frac{1 - v_\theta}{v_\theta}\right), \quad \delta \in I_\delta.$$

We proceed by perturbing the solution V on its equilibrium point

$$V = V_{eq} + \widetilde{V}, \quad \left|\widetilde{V}\right| \ll |V_{eq}|$$

we thus get

$$\frac{\mathrm{d}}{\mathrm{d}\tau}\widetilde{V} = C\widetilde{V}, \quad C = \frac{\partial F}{\partial V}(V_{eq}, \delta)$$

approximating Eq. (A.8) around $V = V_{eq}$. If $C < 0$, then the equilibrium point $g(\delta)$ (with δ given) is hyperbolically stable, while hyperbolically unstable if $C > 0$ (Perko, 2000). $C = 0$ corresponds to an equilibrium point which is not hyperbolic and the nonlinearities must be taken into account. The values of C is

$$\begin{aligned} C &\approx \frac{\partial F}{\partial V}(v_\theta + \delta v_1, \delta) \\ &= \frac{\partial f}{\partial V}(v_\theta + \delta v_1, \delta) - \delta \frac{\partial \psi}{\partial V}(v_\theta + \delta v_1, \delta) \\ &= v_\theta(1 - v_\theta) + \mathcal{O}(\delta) \end{aligned}$$

Hence if $0 < v_\theta < 1$, then $g(\delta)$ is an unstable hyperbolic equilibrium point. Further from the Hartman - Grobman theorem (see for example Perko (2000)) we know that a local hyperbolic equilibrium point of Eq. (A.8) is locally topologically conjugate to its linearizion $\widetilde{V}_\tau = C\widetilde{V}$.

A.3 Asymptotes of the spatial independent NFL model

As discussed in Appendix A.1 and Appendix A.2 the system

$$\begin{aligned} V_\tau &= -(V - v_\theta)(V - 1)V \\ V(0) &= \frac{1}{2}(1 + \tanh(\beta(u_0 - u_\theta))) \end{aligned} \tag{A.10}$$

is a leading order approximation of Eq. (A.4) for large steepness parameters. The scaled threshold value parameter $v_\theta = \frac{u_\theta}{\omega}$ is an equilibrium point of Eq. (A.10) and plays the role as a control parameter. The asymptotic evolution of V and the corresponding asymptotic evolution of the solution u of Eq. (5.11) is presented in Table A.11.

v_θ	u_0	$V(\tau \to \infty)$	$u(t \to \infty)$
$u_\theta < \omega$	$u_0 < u_\theta$	0	0
$u_\theta < \omega$	$u_0 > u_\theta$	1	ω
$u_\theta > \omega$	—	0	0

(A.11)

Table A.11: Overview of the asymptotic behavior of the solution V of Eq. (A.10) and u of Eq. (5.11). Here $v_\theta = \frac{u_\theta}{\omega}$. The initial condition u_0 the firing threshold u_θ and the connectivity ω are given in Eq. (5.11).

A short justification of the above results: since $0 \leq V \leq 1$ the function $-(V - v_\theta)(V - 1)V$ is positive for $V(0) > v_\theta = \frac{u_\theta}{\omega}$ and thus V is a monotonically increasing function, this condition is given as

$$\frac{1}{2}(1 + \tanh(\beta(u_0 - u_\theta))) > \frac{u_\theta}{\omega}. \tag{A.12}$$

Equation (A.12) is true for $u_0 > u_\theta$ and gives $u_\theta < \omega$. For Eq. (5.11) we get

$$\begin{aligned} \frac{\mathrm{d}u}{\mathrm{d}t} &= -u + \omega S(\beta(u - u_\theta)) > 0 \\ &= -u + \omega,\ t \to \infty \end{aligned}$$

We thus get $u(t) = \omega + (u_0 - \omega)\mathrm{e}^{-t} = \omega,\ t \to \infty$.

Appendix B Theorems and definitions

B.1 The contraction mapping theorem

Theorem B.1. *Let $(X_T, ||\cdot||_T)$ be a non-empty complete metric space and $A : (X_T, ||\cdot||_T) \mapsto (X_T, ||\cdot||_T)$ be a contraction mapping of $(X_T, ||\cdot||_T)$, i.e. there is a nonnegative real number $K < 1$ such that*

$$||Au - Av||_T \leq K\,||u - v||_T \;\forall\, u, v \in X_T.$$

Then there exists a unique solution u^* of the equation

$$u^* = Au^*$$

The proof is omitted, instead we refer the reader to Trench (2003)[Thm. 8.3.10].

B.2 Differentiation of integral equations

Theorem B.2. *Let $F : \mathbb{R} \to \mathbb{R}$ be given as*

$$F(t) = \int_a^t f(t,s)\,\mathrm{d}s, \tag{B.1}$$

where f is a continuous differentiable function for all $s, t \in \mathbb{R}$ and well defined for $f(t,t)$. Assume uniform convergence of the integral $\int_a^t [f(t+h,s) - f(t,s)]\,\mathrm{d}s$, where $h > 0$. Then the derivative of F is given as

$$\frac{\mathrm{d}F}{\mathrm{d}t}(t) = \int_a^t \frac{\partial f}{\partial t}(t,s)\,\mathrm{d}s + f(t,t)$$

Proof. Consider the difference given as

$$\begin{aligned}
\frac{F(t+h) - F(t)}{h} &= \frac{1}{h}\left(\int_a^{t+h} f(t+h,s)\,\mathrm{d}s - \int_a^t f(t,s)\,\mathrm{d}s\right) \\
&= \frac{1}{h}\left(\int_a^t f(t+h,s)\,\mathrm{d}s + \int_t^{t+h} f(t+h,s)\,\mathrm{d}s - \int_a^t f(t,s)\,\mathrm{d}s\right) \\
&= \frac{1}{h}\left(\int_a^t [f(t+h,s) - f(t,s)]\,\mathrm{d}s + \int_t^{t+h} f(t+h,s)\,\mathrm{d}s\right)
\end{aligned}$$

Then by the mean value theorem for integrals (see Theorem B.3) where $t^* \in [t, t+h]$ and the limit definition of the derivative we get

$$\begin{aligned}
\frac{\mathrm{d}F}{\mathrm{d}t}(t) &= \lim_{h\to 0} \frac{1}{h} \int_a^t [f(t+h,s) - f(t,s)]\,\mathrm{d}s + f(t+h,t^*) \\
&= \int_a^t \frac{\partial f}{\partial t}(t,s)\,\mathrm{d}s + f(t,t)
\end{aligned}$$

□

The following theorems are adapted from Trench (2003).

B.3 Mean value theorem for integrals

Theorem B.3. *Let f be a continuous real function on the closed interval $[a, b]$ and g is non negative and integrable on $[a, b]$, then there exists a real number $c \in [a, b]$ such that*

$$\int_a^b f(x)g(x)\,\mathrm{d}x = f(c)\int_a^b g(x)\,\mathrm{d}x.$$

B.4 Mean value theorem

Theorem B.4. *Let $f : [a, b] \to \mathbb{R}$ be a continuous function on the closed interval $[a, b]$ and differentiable in the open interval (a, b) where $a < b$. Then*

$$\frac{\mathrm{d}}{\mathrm{d}x}f(c) = \frac{f(b) - f(a)}{b - a},$$

for some real number $c \in (a, b)$

B.5 Taylors theorem

Theorem B.5. *If f and its first n derivatives $f', f'', ..., f^{(n)}$ are continuous on the closed interval $\hat{I}$ between a and b, and $f^{(n)}$ is differentiable on the open interval I between a and b, then there exists a number c between a and b such that*

$$f(b) = f(a) + f'(a)(b-a) + \frac{f''(a)}{2!}(b-a)^2 + \frac{f'''(a)}{3!}(b-a)^3 + \frac{f^{(n)}(a)}{n!}(b-a)^n + \frac{f^{(n+1)}(c)}{(n+1)!}(b-a)^{n+1}$$

where we call the last part the remainder of order n or the error term

$$R_n = \frac{f^{(n+1)}(c)}{(n+1)!}(b-a)^{n+1}$$

This may be rewritten to

$$f(b) - \sum_{n=0}^{r}\frac{f^{(r)}(a)}{r!}(b-a)^r = \frac{f^{(n+1)}(c)}{(n+1)!}(b-a)^{n+1}$$

Remark B.1. If $\lim_{n\to\infty} R_n = 0 \,\forall\, x \in I$ the Taylor series converges

Remark B.2. If $n = 0$ Taylors theorem reduces to the mean value theorem B.4

B.6 Lipschitz continuity

Definition B.1. *This definition is adapted from Perko (2000). Let G be a open subset of $\mathbb{R}^n$. A function $f : G \to \mathbb{R}^n$ is said to be Lipschitz continuous on G if it there is a positive constant λ such that for all $\boldsymbol{x}_2, \boldsymbol{x}_1 \in G$*

$$|f(\boldsymbol{x}_2) - f(\boldsymbol{x}_1)| \leq \lambda\,|\boldsymbol{x}_2 - \boldsymbol{x}_1|$$

The function f is said to be locally Lipschitz on E for each point $\boldsymbol{x}_0 \in G$ if there is an ϵ-neighbourhood of $\boldsymbol{x}_0$, $N_\epsilon \subset G$ and a constant λ_0 such that for all $\boldsymbol{x}_2, \boldsymbol{x}_1 \in N_\epsilon$

$$|f(\boldsymbol{x}_2) - f(\boldsymbol{x}_1)| \leq \lambda_0\,|\boldsymbol{x}_2 - \boldsymbol{x}_1|$$

By an ϵ-neighbourhood of a point $\boldsymbol{x}_0 \in \mathbb{R}^n$ we mean an open ball of positive radius ϵ, i.e

$$N_\epsilon(\boldsymbol{x}_0) = \{\boldsymbol{c} \in \mathbb{R}^n; |\boldsymbol{x} - \boldsymbol{x}_0| < \epsilon\}$$

If for all $\boldsymbol{x}_2, \boldsymbol{x}_1 \in \mathbb{R}^n$ the function f satisfies the following inequality

$$|f(\boldsymbol{x}_2) - f(\boldsymbol{x}_1)| \leq \Lambda\,|\boldsymbol{x}_2 - \boldsymbol{x}_1|$$

the function is said to be globally Lipschitz

Appendix C Python code

In all the below scripts we have imported the following modules:

Python code

```
from __future__ import division
from pylab import *
import odespy
```

Further, we define the python firing-rate function as presented in Eq. (5.1):

Python code

```
def S(u, b, h, a=np):
    return (a.tanh(b * (u - h)) + 1)/2
```

C.1 Convergence estimates of a spatially independent model

The following script was employed in order to measure the numerical error dependency of the steepness parameter β as presented in Section 5.3.2.

Python code

```
def solver(u0, b1, b2, db, T=.001, dt=.00001, h=.6, w=1.):# u0 < w!!

    def f(u, t, b, h, w):
        return (tanh(b * (u - h)) + 1)/2 - u

    dt_e = 1e-7
    nt = int(T/dt)
    nt_e = int(T/dt_e)
    print 'nt = ', nt
    print 'nt_e = ', nt_e
    t_mesh = linspace(0, nt*dt, nt+1)
    t_mesh_exact = linspace(0, nt_e*dt_e, nt_e+1)
    e = []
    Ue_l = []
    U_l = []
    for b in arange(b1,b2,db):
        #approx
        solver1 = odespy.Euler(f, f_kwargs=dict(b=b, h=h, w=w))
        solver1.set_initial_condition(u0)
        U, t = solver1.solve(t_mesh)
        #exact
        solver2 = odespy.RK4(f, f_kwargs=dict(b=b, h=h, w=w))
        solver2.set_initial_condition(u0)
        Ue, t = solver2.solve(t_mesh_exact)

        e.append(abs(U[-1] - Ue[-1]))
        Ue_l.append(Ue)
        U_l.append(U)

    e = array(e)
    return e, U_l, Ue_l, t_mesh, t_mesh_exact
```

The relative error was computed in the following way:

Python code

```
e = ee/(Ue_l[:,-1]*t[-1])
x1 = np.arange(b1,b2,db)
popt, func = curvefit(x1, array(e), guess=[.09,.05,.022])
```

Here ee is the absolute error and Ue_l is a list containing time series for each $\beta \in I_\beta$ with a given $\Delta\beta$.

C.2 Nonlinear curve fit

The non linear curve fit of the numerical error as presented in Section 5.3.2 was computed by the Levenberg Marquard algorithm employed by the SciPy package in the following script.

Python code

```
from scipy.optimize import curve_fit
def curvefit(bs, e, lin_fit=False, guess=False):
    if lin_fit:
        def func(x, a, b, c):
            return b*x + c
    else:
        def func(x, a, b, c):
            return a*np.exp(b*x) + c

    x = linspace(0,bs[-1]-bs[0],len(bs))
    #x = bs
    if guess:
        popt, pcov = curve_fit(func, x, e, p0=guess)
    else:
        popt, pcov = curve_fit(func, x, e)
    print popt
    return popt, func
```

C.3 System of two populations

We begin by defining the following python function, as presented in Eq. (5.23):

Python code

```
def f(u, t, S, wrr, wrs, wss, wsr, h, b):
    r, s = u
    return [-r + (wrr * S(r,b,h) + wrs * S(s,b,h)), -s + (wsr * S(r,b,h) + wss
       * S(s,b,h))]
```

Further, we define a solver function based on the RK4 solver from ODEspy:

Python code

```
def solver(r0,  s0, S, wrr, wrs, wss, wsr, h, b, dt=0.01, T=1.):
    solv = odespy.RK4(f, f_kwargs=dict(S=S, wrr=wrr, wrs=wrs, wss=wss,
       wsr=wsr, h=h, b=b))
    solv.set_initial_condition([r0, s0])
    nt = int(T/dt)
    t_mesh = linspace(0, nt*dt, nt+1)
    u, t = solv.solve(t_mesh)
    r = u[:,0]
    s = u[:,1]
    return r, s, t
```

Thus, by running the following script we produce the results from Section 5.4:

Python code

```
fig = figure()
ax = fig.gca()
s0=.615; r0=.5; wrr=-30; wrs=20; wss=5; wsr=-6; h=.6; b=50
Dt=[0.06, 0.0001]; T=Dt[0]*10; r_list=[]; s_list=[]; t_list=[]
for dt, ls, c in zip(Dt, ['-', '--'],[('g','b'), ('k','r')]):
    r, s, t = solver(r0, s0, S, wrr, wrs, wss, wsr, h, b, dt=dt, T=T)
    r_list.append(r); s_list.append(s); t_list.append(t)
```

References

Amari, S.-I. (1975). Homogeneous nets of neuron-like elements. *Biological Cybernetics*, 17(4):211–220.

Amari, S.-I. (1977). Dynamics of pattern formation in lateral-inhibition type neural fields. *Biological cybernetics*, 27(2):77–87.

Bressloff, P. C. (2012). Spatiotemporal dynamics of continuum neural fields. *Journal of Physics A: Mathematical and Theoretical*, 45(3):033001.

Bressloff, P. C. (2014). Waves in neural media. *AMC*, 10:12.

Coombes, S. (2005). Waves, bumps, and patterns in neural field theories. *Biological Cybernetics*, 93(2):91–108.

Coombes, S. (2006). Neural fields. *Scholarpedia*, 1(6):1373. revision nr. 138631.

Coombes, S. and Schmidt, H. (2010). Neural fields with sigmoidal firing rates: approximate solutions. *Discrete and Continuous Dynamical Systems. Series S*.

Darmofal, D. L. (2005). Computational methods in aerospace engeneering. *MIT open courseware, URL* `http://ocw.mit.edu/courses/aeronautics-and-astronautics/16-901-computational-methods-in-aerospace-engineering-spring-2005/lecture-notes/`. (Accessed 12 April 2014).

Ermentrout, B. (1998). Neural networks as spatio-temporal pattern-forming systems. *Reports on progress in physics*, 61(4):353.

Ermentrout, G. B. and McLeod, J. B. (1993). Existence and uniqueness of travelling waves for a neural network. *Proceedings of the Royal Society of Edinburgh: Section A Mathematics*, 123(03):461–478.

Faye, G. and Faugeras, O. (2010). Some theoretical and numerical results for delayed neural field equations. *Physica D: Nonlinear Phenomena*, 239(9):561–578.

Gerstner, W. and Kistler, W. M. (2002). *Spiking neuron models: Single neurons, populations, plasticity*. Cambridge university press.

Hodgkin, A. L. and Huxley, A. F. (1952). A quantitative description of membrane current and its application to conduction and excitation in nerve. *The Journal of physiology*, 117(4):500.

Hunter, J. D. (2007). Matplotlib: A 2d graphics environment. *Computing In Science & Engineering*, 9(3):90–95.

Iserles, A. (1990). Stability and dynamics of numerical methods for nonlinear ordinary differential equations. *IMA journal of numerical analysis*, 10(1):1–30.

Iserles, A. (2009). *A first course in the numerical analysis of differential equations*, volume 44. Cambridge University Press, 2nd edition.

Jones, E., Oliphant, T., Peterson, P., et al. (2001). SciPy: Open source scientific tools for Python.

Laing, C. R. and Troy, W. C. (2003). Pde methods for nonlocal models. *SIAM Journal on Applied Dynamical Systems*, 2(3):487–516.

Langtangen, H. P. and Wang, L. (2013). The odespy package.

Nielsen, B. F., Shiau, L., and Wyller, J. (2013). Stability analysis of the initial value problem for the wilson-cowan model.

Oleynik, A., Ponosov, A., and Wyller, J. (2013). On the properties of nonlinear nonlocal operators arising in neural field models. *Journal of Mathematical Analysis and Applications*, 398(1):335–351.

Pérez, F. and Granger, B. E. (2007). IPython: a system for interactive scientific computing. *Computing in Science and Engineering*, 9(3):21–29.

Perko, L. (2000). *Differential equations and dynamical systems*, volume 7. Springer.

Petersen, C. C. (2007). The functional organization of the barrel cortex. *Neuron*, 56(2):339 – 355.

Potthast, R. and Beim Graben, P. (2010). Existence and properties of solutions for neural field equations. *Mathematical Methods in the Applied Sciences*, 33(8):935–949.

Shampine, L. F. and Thompson, S. (2007). Stiff systems. *Scholarpedia*, 2(3):2855. revision nr. 139228.

Sobolev, V. I. (originator). Non-linear operator. *Encyclopedia of Mathematics, URL* `http://www.encyclopediaofmath.org/index.php?title=Non-linear_operator&oldid=14292`. (Accessed 12 February 2014).

Sterratt, D., Graham, B., Gillies, A., and Willshaw, D. (2011). *Principles of computational modelling in neuroscience*. Cambridge University Press.

Stuart, A. (1995). Numerical analysis of dynamical systems. *Acta Numerica*.

SymPy Development Team (2014). *SymPy: Python library for symbolic mathematics*.

Trench, W. F. (2003). *Introduction to real analysis*. Prentice Hall/Pearson Education.

Wilson, H. R. and Cowan, J. D. (1972). Excitatory and inhibitory interactions in localized populations of model neurons. *Biophysical journal*, 12(1):1–24.

Wilson, H. R. and Cowan, J. D. (1973). A mathematical theory of the functional dynamics of cortical and thalamic nervous tissue. *Kybernetik*, 13(2):55–80.

Norges miljø- og
biovitenskapelige
universitet

Postboks 5003
NO-1432 Ås
67 23 00 00
www.nmbu.no